



Review

# Design and Application of Electrochemical Sensors with Metal–Organic Frameworks as the Electrode Materials or Signal Tags

Yong Chang<sup>1,2</sup>, Jiaxin Lou<sup>1</sup>, Luyao Yang<sup>1</sup>, Miaomiao Liu<sup>1</sup>, Ning Xia<sup>1</sup> and Lin Liu<sup>1,\*</sup> <sup>1</sup> College of Chemistry and Chemical Engineering, Anyang Normal University, Anyang 455000, China<sup>2</sup> School of Chemistry and Materials Engineering, Jiangnan University, Wuxi 214122, China

\* Correspondence: liulin@aynu.edu.cn

**Abstract:** Metal–organic frameworks (MOFs) with fascinating chemical and physical properties have attracted immense interest from researchers regarding the construction of electrochemical sensors. In this work, we review the most recent advancements of MOF–based electrochemical sensors for the detection of electroactive small molecules and biological macromolecules (e.g., DNA, proteins, and enzymes). The types and functions of MOF–based nanomaterials in terms of the design of electrochemical sensors are also discussed. Furthermore, the limitations and challenges of MOF–based electrochemical sensing devices are explored. This work should be invaluable for the development of MOF–based advanced sensing platforms.

**Keywords:** metal–organic frameworks; electrochemical sensors; small molecules; biomarkers; signal amplification



**Citation:** Chang, Y.; Lou, J.; Yang, L.; Liu, M.; Xia, N.; Liu, L. Design and Application of Electrochemical Sensors with Metal–Organic Frameworks as the Electrode Materials or Signal Tags. *Nanomaterials* **2022**, *12*, 3248. <https://doi.org/10.3390/nano12183248>

Academic Editor: Dong-Joo Kim

Received: 1 September 2022

Accepted: 15 September 2022

Published: 19 September 2022

**Publisher's Note:** MDPI stays neutral with regard to jurisdictional claims in published maps and institutional affiliations.



**Copyright:** © 2022 by the authors. Licensee MDPI, Basel, Switzerland. This article is an open access article distributed under the terms and conditions of the Creative Commons Attribution (CC BY) license (<https://creativecommons.org/licenses/by/4.0/>).

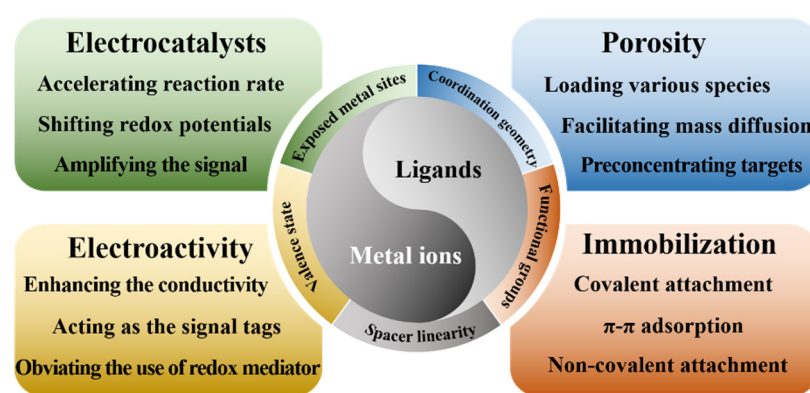
## 1. Introduction

More and more researchers are now committed to developing various novel methods for the detection of inorganic ions, organic pollutants, and biomarkers with the help of fluorescence, colorimetry, surface-enhanced Raman spectroscopy, electrochemistry, electrochemiluminescence, and photoelectrochemistry [1–3]. In contrast to the traditional analytical techniques of mass spectrometry and high-performance liquid chromatography, these methods offer the inherent merits of simple operation and high sensitivity. Among them, electrochemical sensors are extensively utilized in the fields of disease diagnosis, food safety, and environmental science due to their advantages of high sensitivity and selectivity, rapid response, low investment, and good portability.

Electrochemical sensing performance can be improved by modifying the electrode surface and integrating various signal-amplified strategies, such as enzyme catalysis, DNA self-assembly, and nanomaterials-assisted amplification [4–7]. Because of their versatile electrical, mechanical, and physiochemical properties, nanomaterials, including graphene, quantum dots (QDs), and metal nanoparticles, have endowed electrochemical sensors with more possibilities in terms of sensitivity, selectivity, and real-time detection. In fact, the modification of an electrode with nanomaterials can not only increase the effective surface area, enhance the conductivity, and provide catalytic sites (e.g., oxidation metal sites and conjugated  $\pi$ -electron systems) but also facilitate the immobilization of biomolecules (e.g., enzymes, antibodies, DNA, and peptides) with the objective of improving the specificity and sensitivity. In addition, when acting as signal labels in bioassays, nanomaterials labeled with biorecognition elements and signal reporters can increase the number of reporters for each recognition event, finally leading to the amplification of the electrochemical signal.

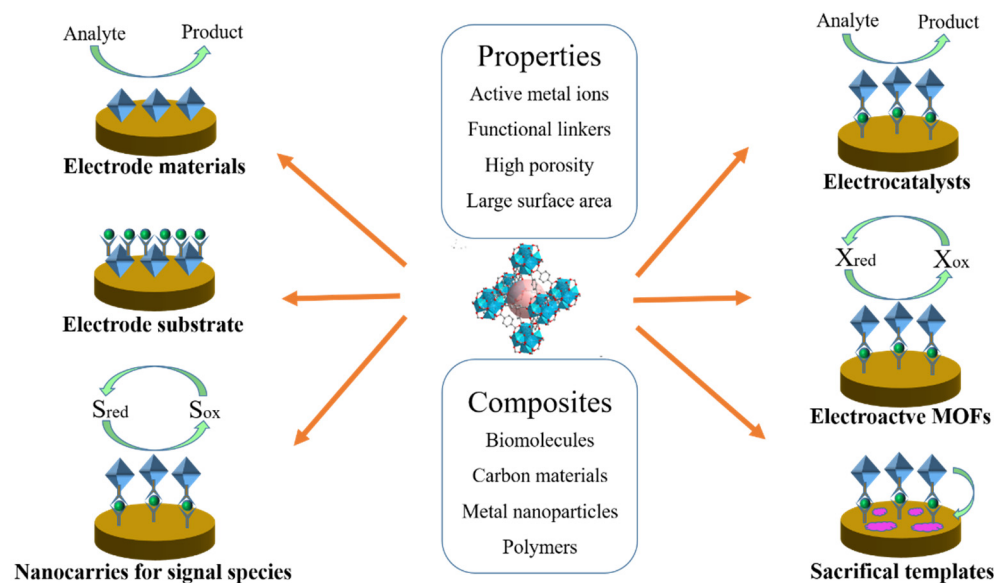
As a novel class of organic–inorganic hybrid crystalline porous coordination polymers, metal–organic frameworks (MOFs) that are self-assembled from metal ions/clusters and

organic ligands exhibit many outstanding properties, including high tunable porosity, good stability, large surface area, and adjustable chemical functionalities [8]. A wide range of building blocks, such as metal ions and organic ligands, can endow MOFs with many effective functions for application in electrochemical assays (Scheme 1). A wide variety of MOFs can be prepared using different approaches, including the solvothermal/hydrothermal method, sonochemical synthesis, electrochemical synthesis, microwave-assisted synthesis, and so on. The advantages of MOFs perfectly match the materials necessary for sensor fabrication [9]. For example, the large surface areas and porous nanostructures of MOFs offer more interfaces and accessible active metal sites by which to catalyze the electrochemical reaction of analysts on the electrode surface [10]. The abundant functional groups and mesoporous properties of MOFs facilitate their functionalization with various materials, including small molecules, antibodies, nucleic acids, enzymes, and nanoparticles. Therefore, MOFs have been used to construct electrochemical sensors with excellent performances in a broad range of potential applications [11–13].



**Scheme 1.** Schematic illustration of the relationship of building blocks (metal ions and ligands) with the functions of MOFs.

The published MOF-based studies have been summarized in previous reviews [14–18]. For example, Li's group and Jouyban's group have reviewed the recent advancements of aptamer-functionalized MOF-based biosensors [19,20]. The preparation and application of MOF-based nanozymes in biosensing and cancer therapy have been reviewed by several groups [21–23]. MOFs can be used as luminescent and electrochemical probes for the detection of biological molecules and cancer biomarkers [24–27]. Wang et al. focused on MOF-based sensing platforms for virus detection [28]. Gorle et al. discussed recent achievements in MOFs-based composites for constructing electrochemical glucose sensors [29]. Wang et al. summarized the recent progress in sensing applications of metal nanoparticles/MOF composites [30]. Mohammadreza's group reviewed the advancement of MOFs in the electrochemical sensing of environmental pollutants [31]. In recent years, MOF-based electrochemical sensors have aroused intense interest. However, there is little in the way of a systematic overview of MOF-based electrochemical sensors using MOFs as the electrode materials or signal tags [32]. Herein, we summarize recent progress in the design and application of MOF-based sensing platforms (Scheme 2). Firstly, we briefly introduce the utilization of pristine MOFs and MOF-based composites as electrode materials for the electrochemical detection of electroactive species. Then, the design and application of MOF-based sensors were discussed, according to the functions of MOFs in the sensing devices. Generally, MOFs can be used as electrode substrates, nanocarriers for signal reporters, electroactive labels, electrocatalysts, and sacrificial templates. Finally, the limitations and challenges of MOF-based sensors are discussed, which is of great significance for exploring new multifunctional MOFs for electrochemical analysis. Due to the explosive growth of academic articles and the highly dynamic development of this topic, some important papers may be omitted during the review period. We sincerely apologize to those authors whose studies were overlooked in this article.



**Scheme 2.** Schematic illustration of the different functions of MOFs and their composites in the construction of electrochemical sensing platforms.

## 2. MOFs as the Electrode Materials of Electrochemical Sensors

MOFs, with unsaturated active sites, tunable pore sizes, and good electrocatalytic activity, can effectively enhance the electrochemical response and increase detection sensitivity. In addition, their high porosity, large surface area, and abundant functional groups are beneficial for concentrating the analytes and improving mass transfer efficiency [33–35]. The specific size and shape of the available cavities and channels can endow MOF-based sensors with relatively high selectivity. However, the inherent characteristics of low chemical stability in aqueous medium and the poor conductivity of MOFs may dramatically hinder their electrochemical applications in practical samples. Aiming to overcome the shortcomings, different conductive materials and nanomaterials have been integrated with pristine MOFs to improve the electrochemical sensing performance [36]. In this section, the advancements of MOFs in sensing electroactive small molecules and metal ions are briefly discussed, based on the types of additional materials that have been used for integration with MOFs.

### 2.1. Pristine MOFs

Inorganic nodes and organic linkers in MOFs play a decisive role in their electrocatalytic performances [37–39]. MOFs have been considered the ideal materials for non-enzymatic electrochemical sensors owing to the redox behavior of metal ions (Table 1) [40,41]. Several small biomolecules (e.g., dopamine (DA), uric acid (UA), ascorbic acid (AA), glucose, H<sub>2</sub>O<sub>2</sub>, and amino acids) have been catalytically oxidized by the active metal sites (e.g., Cu<sup>2+</sup>, Co<sup>2+</sup>, Cr<sup>2+</sup>, Zn<sup>2+</sup>, and Ni<sup>2+</sup>) in MOFs [42–44]. For example, Cu-based pristine MOFs could be used to detect small molecules due to the rapid electron transfer process of Cu(II)–MOF/Cu(I)–MOF couple. Moallem et al. prepared Cu-benzene-1,3,5-tricarboxylic acid (Cu–BTC) MOFs by the ultrasound-assisted hydrothermal method and used the composites to modify a carbon paste electrode (CPE) for the simultaneous detection of DA and UA [45]. Li et al. reported a Cr–MOF-based electrochemical sensor for the simultaneous determination of DA and UA [46]. The large pore volume of Cr–MOFs provided plenty of active sites to catalyze the oxidation of DA and UA, leading to an increased peak separation value. Co–MOFs with peroxidase-like activity have also been used as active substrates for the electrocatalytic reduction of H<sub>2</sub>O<sub>2</sub> [47].

Environmental pollutants (e.g., pesticides, heavy metal ions, phenolics, and toxins) are harmful to both the environment and human health. MOF-based electrochemical sensors have been extensively developed for the analysis of environmental pollutants [48–50].

For example, Cu–TCPP and Cu–BTC were used as electrode modifiers to construct electrochemical sensors for the detection of glyphosate [51,52]. Hu et al. reported a Cu–MOFs–based sensor for the detection of carbendazim in water [53]. Dong et al. developed an electrochemical sensor for 2,4-dichlorophenol, based on Cu–BTC MOFs [54]. Heavy metal ions in natural resources are harmful to living organisms. Because of their characteristics of a large surface area, high porosity, and tunable chemical functionality, MOFs modified at the electrode can act as concentrators to accelerate the preconcentration process of anodic stripping voltammetry (ASV), improving the detection sensitivity [55,56]. For example, Guo et al. developed an electrochemical sensor for  $\text{Pb}^{2+}$  detection using amino-functionalized Ni–MOFs [57]. The fern-leaf-like MIL-47(as) was used to develop an electrochemical sensor for the simultaneous detection of  $\text{Pb}^{2+}$ ,  $\text{Cu}^{2+}$ , and  $\text{Hg}^{2+}$  [58]. In addition, Guo et al. reported an electrochemical sensor for  $\text{Pb}^{2+}$  detection created by using amino-functionalized Ni(II)–based MOFs to modify the electrode [57].  $\text{Pb}^{2+}$  was absorbed by the amino group of a 2-aminobenzenedicarboxylic acid ( $\text{NH}_2$ –BDC) linker, leading to an increase in the current intensity. The Ni–MOFs–modified electrode showed excellent selectivity toward  $\text{Pb}^{2+}$ , due to the ion size exclusion.

Compared with monometallic MOFs, bimetallic MOFs with an optimized ratio of metal ions exhibit higher electrical conductivity, stability, and catalytic efficiency [59,60]. Bimetallic MOFs (e.g., Cu–Co–MOFs, Zn–Ni–MOFs, and Co–Ni–MOFs) have been used to develop enzyme-free electrochemical sensors for the detection of various targets, including glucose, adenosine, organophosphate, bisphenol A (BPA), and so on [61–64]. Typically, Huang et al. developed a three-dimensional (3D) Co–doped Ni–based conductive MOFs–modified electrochemical sensor for the detection of L-tryptophan (Trp) [65]. Co–Ni–MOFs showed high catalytic activity toward Trp oxidation due to the porous structure, larger surface area, and more active sites in the redox process. The proposed sensor for Trp detection achieved a wide linear range from 0.01 to 300  $\mu\text{M}$  and a low limit of detection (LOD) (8.7 nM). Compared to the conventional 3D MOFs, 2D MOFs are more attractive because of their outstanding advantages of larger surface area/volume ratio, easier diffusion, and more available active sites for catalysis. Li et al. fabricated an ultrathin Ni–MOF nanosheet-based assembly for the detection of AA (Figure 1A) [66]. The nanosheet, with a uniform thickness of 8 nm, facilitated the interaction between MOF and AA. The Ni–MOF nanosheet-modified electrode exhibited a satisfactory linear range from 0.5  $\mu\text{M}$  to 8065.5  $\mu\text{M}$  and an LOD of 0.25  $\mu\text{M}$ . Wang et al. prepared a series of Co, Cu, and Zn-based ultrathin 2D bimetallic MOF nanosheets using Fe(III) tetra(4-carboxyphenyl)porphine chloride (TCPP(Fe)) as the ligand (Figure 1B) [67]. The MOF nanosheets obtained by the surfactant-assisted method formed a multilayer film on the electrode surface. The modified electrode was used for the sensitive detection of  $\text{H}_2\text{O}_2$  secreted by live cells.

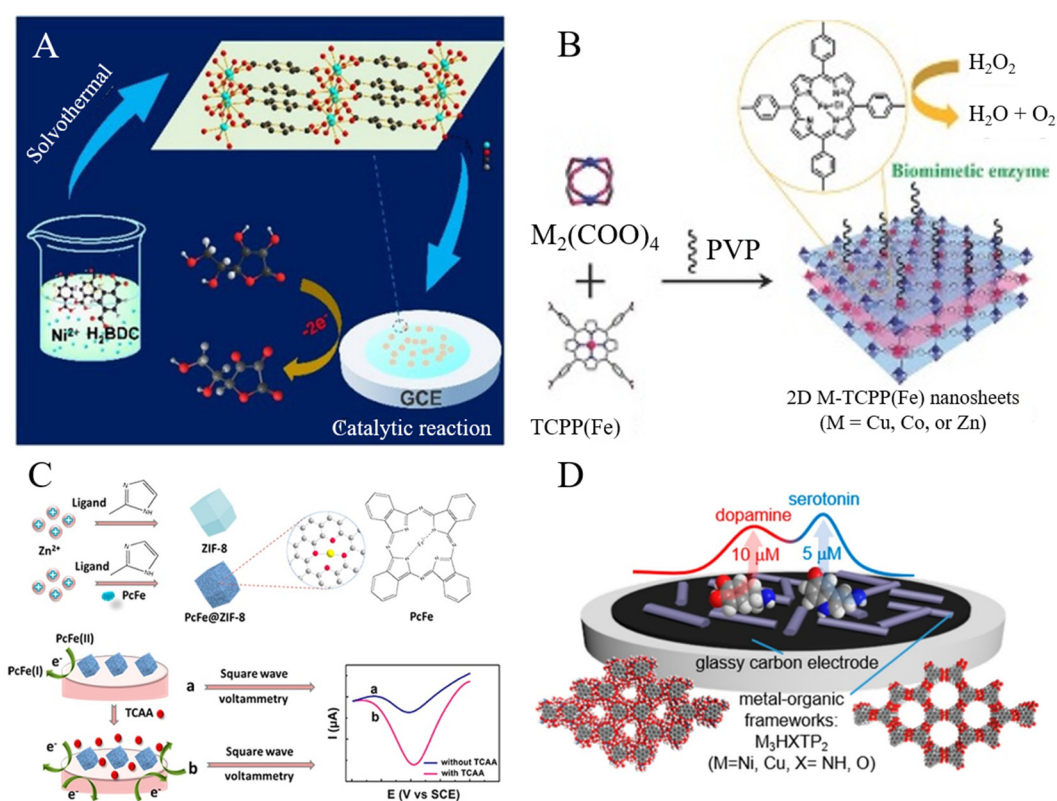


**Figure 1.** (A) Schematic illustration of the synthesis of the Ni–MOF and the Ni–MOF applied for catalyzing AA. Reprinted with permission from Ref. [66]. Copyright 2018, Wiley-VCH. (B) Schematic illustration of two-dimensional bimetallic MOF nanosheets applied for catalyzing  $\text{H}_2\text{O}_2$ . Reprinted with permission from Ref. [67]. Copyright 2016, Wiley-VCH. (C) Schematic illustration of ZIF-8 and PcFe@ZIF-8 synthesis process and the electrochemical sensing mechanism for TCAA determination. Reprinted with permission from Ref. [68]. Copyright 2019, American Chemical Society. (D) Schematics of 2D layered conductive MOFs–based electrochemical sensor for TCAA determination. Reprinted with permission from Ref. [69]. Copyright 2020, American Chemical Society.

Porphyrins with stable and rigid structures, coordinated with different metal ions, can be used as electrocatalytic sites in a metal-binding or metal-free state [70]. Porphyrinic MOFs with excellent enzyme-mimicking catalytic activity have been utilized for the electrochemical detection of nitroaromatic compounds, nitrite, UA,  $\text{H}_2\text{O}_2$ , and so on [71–75]. For example, Kung et al. demonstrated that the zirconium-based porphyrin MOF (MOF–525) thin-film-modified electrode showed high conductivity and electrocatalytic activity for nitrite oxidation [76]. In view of the fast redox reaction and high catalytic activity of iron phthalocyanine (PcFe), Zeng et al. reported the detection of trichloroacetic acid (TCAA) using PcFe– and Zn–based MOF (ZIF-8) composites as the electrode materials (Figure 1C) [68]. In this method, PcFe(II) was first electrochemically reduced into PcFe(I), then the produced PcFe(I) was immediately re-oxidized by TCAA. Based on the redox cycling, TCAA has been determined with an LOD of 1.89 nM. Moreover, hexasubstituted triphenylene with good electrical conductivity has been used to prepare conductive MOFs. Ko et al. prepared an electrochemical sensor for the detection of redox-active neurochemicals using the 2D layered conductive MOFs–casted electrode, including AA, DA, UA, and serotonin (5-HT) (Figure 1D) [69]. Among the conductive MOFs,  $\text{M}_3\text{HXTp}_2$  (M = Ni, Cu; and X = NH, 2,3,6,7,10,11-hexaiminotriphenylene (HITP) or O,2,3,6,7,10,11-hexahydroxytriphenylene (HHTP)), the  $\text{Ni}_3\text{HHTP}_2$  MOFs exhibited the best sensing performances and could be used for the detection of 63 nM DA and 40 nM 5-HT, with a wide linear range. The sensor was further used for the determination of 5-HT in simulated urine.

**Table 1.** Detection performances of pristine MOF-based electrochemical sensors.

Electrode Material	Analyte	Linear Range	LOD	Ref.
Zn <sub>4</sub> O(BDC) <sub>3</sub> (MOF-5)	Pb <sup>2+</sup>	10 nM~1.0 μM	4.9 nM	[33]
TMU-16-NH <sub>2</sub> (Zn)	Cd <sup>2+</sup>	62.5 nM~1.1 μM	1.8 nM	[34]
[H <sub>2</sub> N(CH <sub>3</sub> ) <sub>2</sub> ] <sub>4</sub> [Zn <sub>3</sub> (Hdpa) <sub>2</sub> ]•4DMF	Cu <sup>2+</sup>	5.0 pM~900 nM	1.0 pM	[35]
Co-MOFs	glucose	1.0 μM~3.0 mM	1.3 nM	[37]
Cu-MOFs	BPA	50 nM~3.0 μM	13 nM	[38]
Cu-BTC	methocarbamol	80 μM~800 μM	50 nM	[39]
Cr-MOFs	H <sub>2</sub> O <sub>2</sub>	25 μM~500 μM	3.52 μM	[40]
Cu-BTC	DA and UA	50 nM~500 μM and 0.5 μM~600 μM	30 and 200 nM	[45]
Cu <sub>3</sub> (BTC) <sub>2</sub>	2,4-dichlorophenol	40 nM~1.0 μM	9.0 nM	[54]
Co-MOFs	H <sub>2</sub> O <sub>2</sub>	5.0 μM~9.0 mM	3.76 μM	[47]
Ni-MOFs	Pb <sup>2+</sup>	0.5 μM~6.0 μM	0.508 μM	[57]
MIL-101(Cr)	DA and UA	5.0~250 μM and 30~200 μM	Not reported	[46]
Co-Ni-MOFs	Trp	10 nM~300 μM	8.7 nM	[65]
Ni-MOFs	AA	0.5 μM~8.1 μM	0.25 μM	[66]
(Co-TCPP(Fe)) <sub>5</sub>	H <sub>2</sub> O <sub>2</sub>	0.4 μM~50 μM	0.15 μM	[67]
MOF-52(Zr)	NO <sub>3</sub> <sup>-</sup>	20 μM~800 μM	2.1 μM	[76]
PcFe@ZIF-8	TCAA	20 nM~1.0 μM	1.89 nM	[68]

**Abbreviations:** BDC, 1,4-dicarboxybenzene; MOFs, metal-organic framework; Hdpa, 3,4-di(3,5-dicarboxyphenyl)phthalic acid; BPA, bisphenol A; BTC, 1,3,5-benzenetricarboxylic acid; DA, dopamine; UA, uric acid; Trp, L-tryptophan; AA, ascorbic acid; TCPP(Fe), Fe(III) tetra(4-carboxyphenyl)porphine chloride; PcFe, iron(II) phthalocyanine; TCAA, trichloroacetic acid.

## 2.2. Carbon Materials-Modified MOFs

Owing to their high conductivity, low cost, and chemical inertness, distinct-dimension carbon materials have been extensively used to prepare hybrid composites with MOFs, including 1D carbon nanotubes (CNT), 2D graphene, and mesoporous carbon [77–79]. CNT is considered to be one of the most promising carbon materials to improve the performance of MOFs because of its unique electrical conductivity, high surface area, and high thermal/mechanical stability [80]. CNT/MOFs composites have been used for the electrochemical detection of a wide range of targets, including gallic acid, opioid drugs, tetracycline, and so on (Table 2) [81–85]. For instance, Li et al. reported an electrochemical sensor for the detection of DA and acetaminophen (ACOP), using the hybrid composite of UiO-66-NH<sub>2</sub> and CNT as the electrocatalyst [86]. Mn-MOFs were grown in situ on multi-walled CNTs (MWCNTs) for the simultaneous detection of AA, DA, and UA in bodily fluids [87]. Moreover, quasi-2D Ni-MOF nanosheets were prepared in situ under the confinement effect of the cross-linked CNT networks; the resulting hybrid composites were applied to detect BPA [88]. Ratiometric electrochemical sensors, based on the ratio of an internal reference signal and a response signal for an analyte, can improve their accuracy and stability. Recently, Rong et al. designed a ratiometric electrochemical sensor for the determination of doxorubicin, based on electroactive methylene blue (MB)-loaded MWCNTs/UiO-66-NH<sub>2</sub> [89]. As shown in Figure 2A, the UiO-66-NH<sub>2</sub> MOFs were synthesized in the presence of MWCNTs and the composites were further used to load a large number of MB molecules. The porous UiO-66-NH<sub>2</sub> could not only catalyze the oxidation of doxorubicin but also facilitate the adsorption of MB as an internal reference. The ratiometric sensor exhibited higher selectivity and stabilization, in contrast to that with a single-signal response.

**Table 2.** The detection performances of carbon nanomaterials-decorated MOF-based electrochemical sensors.

Electrode Material	Analyte	Linear Range	LOD	Ref.
MIL-101(Cr)@rGO	4-nonylphenol	100 nM~12.5 $\mu$ M	33 nM	[90]
Cu-hemin MOF/CS-rGO	H <sub>2</sub> O <sub>2</sub>	65 nM~0.41 mM	19 nM	[91]
Cu(tpa)-EGR	ACOP and DA	1.0 $\mu$ M~100 $\mu$ M and 1.0 $\mu$ M~50 $\mu$ M	0.36 and 0.21 $\mu$ M	[92]
Co-MOF/BP-RGO	chlorogenic acid	1.0 nM~391 $\mu$ M	14 nM	[93]
PPy@ZIF-8/GAs	dichlorophenol	10 nM~10 $\mu$ M	0.1 nM	[94]
GA-UiO-66-NH <sub>2</sub>	Cd <sup>2+</sup> , Pb <sup>2+</sup> , Cu <sup>2+</sup> , and Hg <sup>2+</sup>	10 nM~1.5 $\mu$ M, 1.0 nM~2.0 $\mu$ M, 10 nM~1.6 $\mu$ M and 1.0 nM~22 $\mu$ M	9.0, 1.0, 8.0 and 0.9 nM	[95]
Ni-MOFs/CNTs	H <sub>2</sub> O <sub>2</sub>	10 $\mu$ M~51.6 mM	2.1 $\mu$ M	[80]
UiO-66-NH <sub>2</sub> /CNTs	DA and AC	30 nM~2.0 $\mu$ M	15 and 9.0 nM	[86]
Mn-BDC@MWCNT	AA, DA and UA	0.1 $\mu$ M~1.15 mM, 10 nM~0.5 mM, and 20 nM~1.1 mM	10, 2.0 and 5.0 nM	[87]
3D Ni-MOF@CNTs	BPA	1.0 nM~1.0 $\mu$ M	0.35 nM	[88]
MB@MWCNTs/UiO-66-NH <sub>2</sub>	doxorubicin	0.1 $\mu$ M~75 $\mu$ M	51 nM	[89]
Co-MOF@MPC	hydrazine and nitrobenzene	5.0 $\mu$ M~0.63 mM and 0.5 $\mu$ M~15 $\mu$ M	1.75 and 0.21 $\mu$ M	[96]
ZIF67-OMC	HQ and catechol	0.1 $\mu$ M~100 $\mu$ M	52 and 36 nM	[97]
DUT-9/MC	Baicalein	50 nM~20 $\mu$ M	15 nM	[98]
pFeMOF/OMC	H <sub>2</sub> O <sub>2</sub>	0.5~70.5 $\mu$ M	0.45 $\mu$ M	[99]
Cu-MOFs/OMC	hydrazine	0.5 $\mu$ M~0.711 mM	0.35 $\mu$ M	[100]
Ag-ZIF-8/OMC	xanthine	1.0 $\mu$ M~0.28 mM	0.167 $\mu$ M	[101]

**Abbreviation:** rGO, reduced graphene oxide; MOFs, metal-organic framework; CS, chitosan; tpa, terephthalate; EGR, electrochemically reduced graphene; ACOP, acetaminophen; PPy, polypyrrole; GA, graphene aerogel; CNTs, carbon nanotubes; MWCNT, multiwall carbon nanotubes; MB, methylene blue; MPC, mesoporous carbon; OMC, ordered mesoporous carbon; HQ, hydroquinone.

Graphene and its analogs have been widely used in the development of electrochemical sensors, owing to its high electrical conductivity, large specific surface area, and excellent chemical stability. A combination of graphene and its analogs with MOFs is an effective approach to increasing the conductivity of MOFs [102,103]. Different hybrid composites of MOFs and graphene analogs (e.g., graphene oxide (GO) aerogel/Cu-MOFs, reduced GO/Cr-MOFs, and graphene/ZIF-67) have been applied to construct sensors for the enzyme-free determination of catechol, 4-nonylphenol, H<sub>2</sub>O<sub>2</sub>, glucose, paraquat, and so on [90,91,104–108]. For example, Wang et al. synthesized the hybrid nanocomposites of copper terephthalate MOF-GO (Cu(tpa)-GO) via an ultrasonication method. The nanocomposites were then used for the determination of drugs (ACOP and DA) [92]. As shown in Figure 2B, the Cu(tpa) was bound with GO through  $\pi$ - $\pi$  stacking, hydrogen bonding, and Cu-O coordination interactions. After being cast on the glass carbon electrode (GCE), the GO in the composite was electrochemically transformed into reduced graphene with a higher accessible surface area and conductivity. The electroactive Cu(tpa) MOFs in the composites showed a positive influence on enhancing the electrochemical response of ACOP and DA. The LOD for DA was 0.21  $\mu$ M and that for AP was 0.36  $\mu$ M. Heteroatom doping can change the electronic structure of GO and improve its electrochemical properties. Recently, Mariyappan et al. developed an electrochemical sensor for chlorogenic acid detection by using Co-MOFs/heteroatoms-doped reduced GO (rGO) [93]. The electron-poor and electron-rich dopants activated the nearby carbon and produced more charged sites for the adsorption of analytes. Moreover, graphene aerogels (GAs) with high porosity and low density offer various sites for binding with MOFs. The combination of MOFs with the GAs matrix can cause a novel synergistic effect for electrochemical sensing [94]. Thus, Lu et al. developed an electrochemical sensor for the simultaneous detection of multiple metal ions in aqueous media by using GAs-supported UiO-66-NH<sub>2</sub> composites to modify the electrode (Figure 2C) [95]. In this work, GAs enhanced the conductivity and accelerated the electron transfer. Moreover, they acted as the backbones for the in situ growth of UiO-66-NH<sub>2</sub>. The large specific surface area (707.79 m<sup>2</sup> g<sup>-1</sup>) and the hierarchical porous

structure of GA-UiO-66-NH<sub>2</sub> provided more active sites and mass-transfer pathways for heavy metal ions.

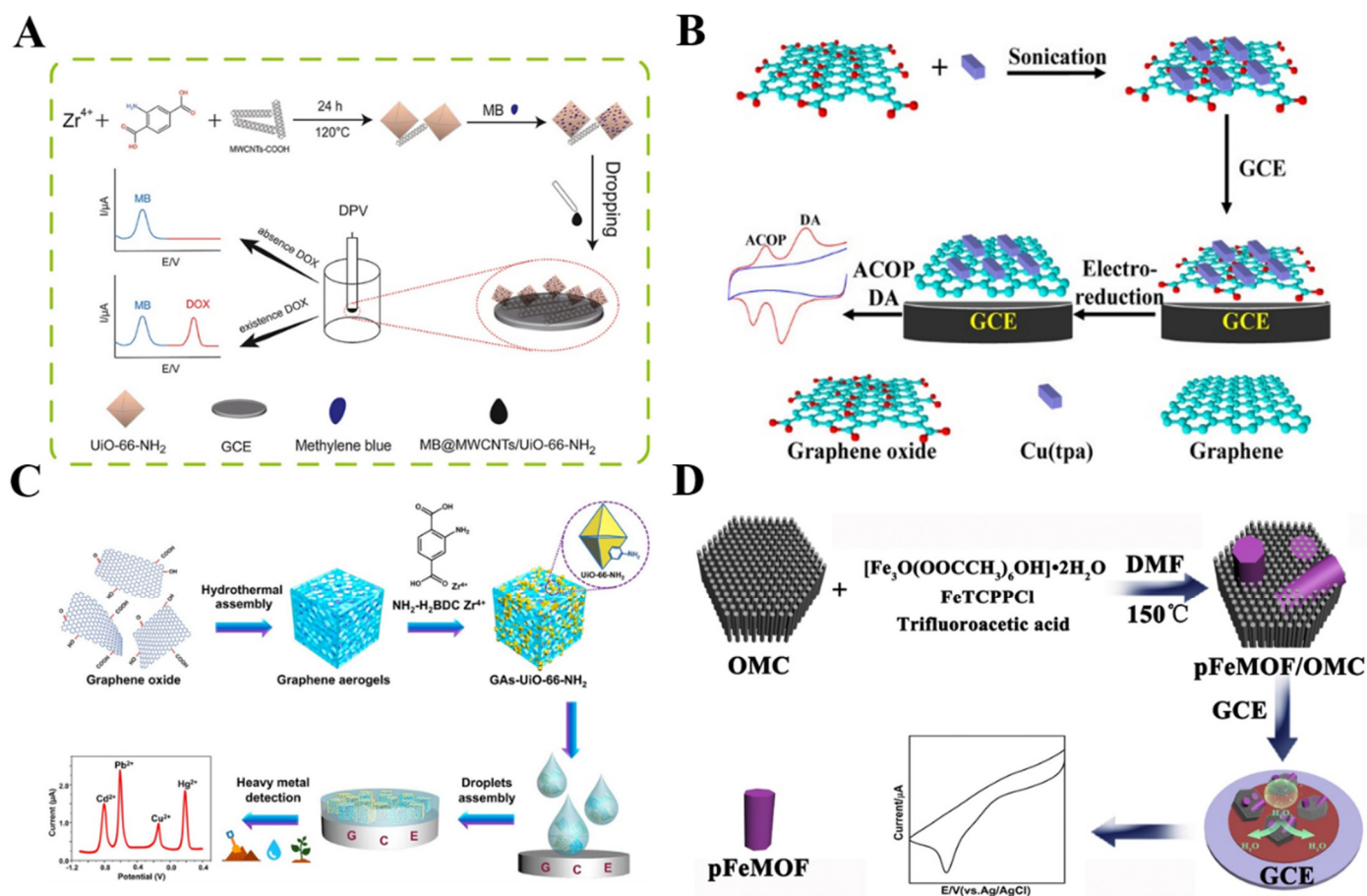


**Figure 2.** (A) Schematic illustration of a ratiometric electrochemical sensor for the determination of doxorubicin, based on MB-loaded MWCNTs/UiO-66-NH<sub>2</sub>. Reprinted with permission from Ref. [89]. Copyright 2022, Elsevier. (B) Schematic illustration of the ultrasonication-assisted preparation of Cu(tpa)-GO and the simultaneous determination of ACOP and DA. Reprinted with permission from Ref. [92]. Copyright 2014, American Chemical Society. (C) Schematic illustration of the preparation of GAs-UiO-66-NH<sub>2</sub> and the simultaneous detection of heavy-metal ions by a GAs-UiO-66-NH<sub>2</sub> modified electrode. Reprinted with permission from Ref. [95]. Copyright 2019, American Chemical Society. (D) Schematic illustration of the preparation pathway of pFeMOF/OMC samples. Reprinted with permission from Ref. [99]. Copyright 2017, Elsevier.

Mesoporous carbon (MC), with large pore volumes and superior adsorption capacity, can also be used as a support platform for MOFs. Different MC/MOFs (e.g., MC/Fe-MOFs, MC/Co-MOFs, and MC/ZIF-8) composite-based electrochemical sensors have been reported for the detection of H<sub>2</sub>O<sub>2</sub>, p-nitrotoluene, hydrazine, pyrazinamide, and isonicotinyl hydrazide [97,98,109–112]. Typically, Deng et al. reported the synthesis in situ of UiO-66 on MC and applied the UiO-66/MC composites to determine the dihydroxybenzene isomers [113]. Zhang et al. demonstrated that the macropores of MC could regulate the homogeneous growth of Co-MOF crystallites, thus providing a large active area for the adsorption of analytes [96]. Ordered MC (OMC), with well-ordered pores, a shorter mesopore channel length, and a large specific surface area can significantly improve the sensitivity of sensors [100,114]. The ZIF-8 and OMC composites were applied to construct an electrochemical sensor for xanthine [101]. In addition, Liu et al. reported the electrochemical detection of H<sub>2</sub>O<sub>2</sub> in living cells by using porphyrinic iron-based MOF (pFeMOF)/OMC (Figure 2D) [99]. OMC restricted the growth of pFeMOF crystallites and reduced the ag-

glomeration of pFeMOF, providing more active sites when they were exposed to  $\text{H}_2\text{O}_2$ . The pFeMOF, self-assembled from  $\text{Fe}^{3+}$  and porphyrin, possessed a peroxidase-mimic catalytic ability and amplified the electrochemical signal by the reduction of  $\text{H}_2\text{O}_2$ .

### 2.3. Noble Metal Nanomaterials

Noble metal nanomaterials, including gold (Au), silver (Ag), and platinum (Pt), have been commonly used as electrocatalysts, to develop various electrochemical sensing devices with high sensitivity and excellent conductivity. The incorporation of precious metal nanomaterials into MOFs can improve the conductivity of MOFs and protect the migration and agglomeration of metal nanomaterials [115]. AuNP–modified MOFs were used to construct an electrochemical sensing platform for the detection of nitrite, methyl mercury species, nitrofurazone, estrone, and DA (Table 3) [116–120]. For example, an AuNP/MOF composite–modified CPE was constructed for the detection of BPA by Silva and co-workers [121]. Mollarasouli et al. prepared porous Cu–MOFs/ZnTe nanorods/AuNPs hybrid composites and used them for the determination of catechol [122]. Wang et al. prepared AuNP–modified MOF (AuNPs/MMPF-6(Fe)) composites via electrostatic interaction and employed them as the electrode materials to detect hydroxylamine with a high electrocatalytic response (Figure 3A) [123]. This work provided a simple method for studying the electrochemical behavior of metalloporphyrin and indicated the potential application of MOF–based composites for bioassays.

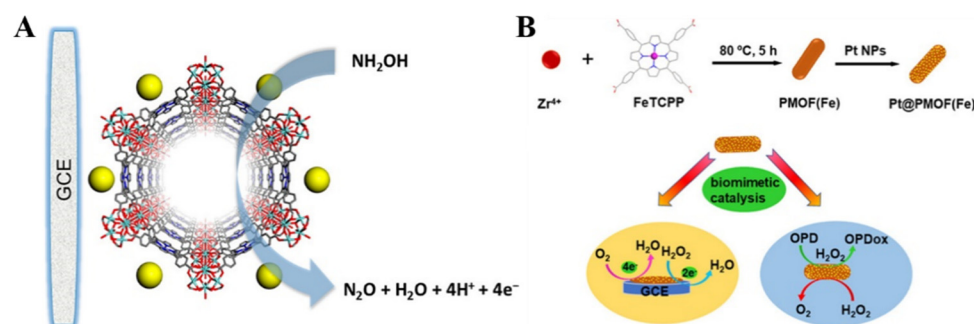


**Figure 3.** (A) Schematic illustration of AuNP–modified MMPF-6(Fe) composites to detect hydroxylamine. Reprinted with permission from Ref. [123]. Copyright 2016, American Chemical Society. (B) Schematic illustration of the preparation of Pt@PMOF(Fe) and the biomimetic catalysis of Pt@PMOF(Fe). Reprinted with permission from Ref. [124]. Copyright 2020, American Chemical Society.

In addition, hybrid composites of silver nanoparticles (AgNPs) and MOFs have been used to develop electrochemical assays for the detection of  $\text{H}_2\text{O}_2$ , nitrite, peracetic acid, glucose, and so on [125–129]. For example, Peng et al. used MIL-101(Fe) MOFs as the carriers to load AgNPs and then fabricated an electrochemical sensor for Trp detection [130]. The results showed that the combination of MIL-101(Fe) and AgNPs accelerated the electron transfer, thus enhancing the oxidation current of Trp. Liu et al. reported the detection of glutathione (GSH) by using AgNPs to decorate flower-like ultrathin Cu-TCPP MOFs nanosheets [131]. The nanocomposites could increase the electrical conductivity and promote the adsorption of GSH on the sensing interface. Under the synergistic electrocatalysis of MOFs and AgNPs, GSH was sensitively determined in a concentration range that varied from 1.0  $\mu\text{M}$  to 100  $\mu\text{M}$ , with a LOD of 66 nM. Recently, Fan et al. prepared ZIF-67/AgNPs/polydopamine (PDA) nanocomposites with a yolk–shell structure and developed a sensor for the detection of  $\text{Cl}^-$  [132]. In this work,  $\text{Ag}^+$  ions were reduced to AgNPs by DA molecules, and the resulting AgNPs were stabilized by the PDA shell on the ZIF-67/AgNPs surface.

**Table 3.** Detection performances of different metal nanoparticle-modified MOF-based electrochemical sensors.

Electrode Material	Analyte	Linear Range	LOD	Ref.
Pt@UiO-66	H <sub>2</sub> O <sub>2</sub>	5.0 μM~14.75 mM	3.06 μM	[115]
Cu-MOF/Au NPs	NO <sub>3</sub> <sup>-</sup>	0.1 μM~4.0 mM	8.2 nM	[116]
AuNPs@Cu-MOF	BPA	0.2~1.0 mM	37.8 μM	[121]
Cu-MOF/ZnTe NRs/Au NPs	catechol	250 nM~0.3 mM	16 nM	[122]
AuNPs/MMPF-6(Fe)	hydroxylamine	0.01~1.0 μM and 1.0~20 μM	4.0 nM	[123]
AgNPs@ZIF-67	H <sub>2</sub> O <sub>2</sub>	5.0 μM~275 μM	1.5 μM	[126]
AgNPs/MIL-101(Fe)	Trp	1.0~50 μM	0.14 μM	[130]
Ag/Cu-TCPP	GSH	1.0~100 μM	66 nM	[131]
ZIF-67/Ag NPs/PDA	Cl <sup>-</sup>	2.0~400 mM	1.0 mM	[132]
Pt@PMOF(Fe)	H <sub>2</sub> O <sub>2</sub>	0~10 mM	6.0 μM	[124]

**Abbreviation:** AuNPs, gold nanoparticles; BPA, bisphenol A; AgNPs, silver nanoparticles; PDA, polydopamine; Trp, L-tryptophan; GSH, glutathione; PANI, polyaniline.

Besides AuNPs and AgNPs, PtNPs were also decorated on the surface of MOFs as a way to develop electrochemical sensors. For example, Ling et al. reported the preparation of metalloporphyrinic PMOF(Fe) through Fe porphyrin-Zr<sup>4+</sup> interaction (Figure 3B) [124]. The resulting Pt@PMOF(Fe), with many active Fe centers and dispersed PtNPs on the surface, endowed the nanocomposites with a large surface area and high catalase- and peroxidase-mimicking activities. The PMOF(Fe) acted as a nanocarrier to hinder the aggregation of PtNPs. The Pt@PMOF(Fe) exhibited high catalytic activity for the electrochemical reduction of H<sub>2</sub>O<sub>2</sub> and O<sub>2</sub>, thus facilitating the design of MOF-based sensing platforms.

#### 2.4. Conductive Polymers

The conductive polymers usually involved in polypyrrole (PPy), polythiophene (PTh), and polyaniline (PANI) have been used to modify MOFs for electrochemical assays, due to their simple preparation, good adhesion, high conductivity, and excellent environmental stability [133,134]. Thus, the polymer/MOF (e.g., PANI/Al-MOFs, PPy/Mo-MOFs, PPy/ZIF-8, and PEDOT/MOF-525) composites were prepared and used to detect various targets, such as Zn<sup>2+</sup>, DA, hydroxylamine, quercetin, and so on (Table 4) [135–139]. For instance, Wang et al. developed an electrochemical sensor for the detection of Cd<sup>2+</sup>, based on PANI-functionalized UiO-66-NH<sub>2</sub> [140]. In the composite, PANI improved the conductivity of MOFs by accelerating the electron transfer. In addition, Xu et al. developed an electrochemical nitrite sensor based on PPy/UiO-66 composites, which were fabricated through in situ oxidative polymerization [141]. The NH<sub>2</sub>-MIL-53(Al) MOFs were electrodeposited on the PPy nanowires and the hybrid nanocomposites were used to modify an electrode for the detection of Pb<sup>2+</sup> and Cu<sup>2+</sup> [142]. Due to their good flexibility, electrocatalytic activity, and ease of doping, poly(3,4-ethylenedioxythiophene) (PEDOT) has also been used to modify MOFs [70]. Wang et al. prepared Ni-MOF/PEDOT hybrid composites for the detection of gallic acid and tinidazole [143]. PEDOT acted as the carrier platform for the in situ growth of MOFs and prevented the aggregation of Ni-MOF.

**Table 4.** Detection performances of different conductive polymer and modified MOF-based electrochemical sensors.

Electrode Material	Analyte	Linear Range	LOD	Ref.
PANI@Al-SA	Zn <sup>2+</sup>	2.8~228.6 μM	0.59 μM	[135]
CuTRZMoO <sub>4</sub> @PPy	DA	1.0~100 μM	80 nM	[136]
ZIF-PEDOT	hydroxylamine	0.1~0.6922 mM	40 nM	[137]
PPy@ZIF-8	quercetin	0.01~7.0 μM and 7.0~150 μM	7.0 nM	[138]
UiO-66-NH <sub>2</sub> @PANI	Cd <sup>2+</sup>	4.5 nM~5.4 μM	2.7 nM	[140]
PPy/UiO-66	NO <sub>3</sub> <sup>-</sup>	50 nM~1.0555 mM	37 nM	[141]

**Abbreviation:** PANI, polyaniline; SA, succinate; PPy, polypyrrole; DA, dopamine; PEDOT, poly(3,4-ethylenedioxythiophene).

### 3. MOFs as Supporting Platforms

For the fabrication of electrochemical biosensors, biomolecules, such as enzymes, DNA, and antibodies are always used as the recognition elements because of their high selectivity, sensitivity, and signal-to-noise ratio. MOFs with large surface areas, high porosity, and good biocompatibility can be used as excellent porous supports for the immobilization of biomolecules on an electrode surface via covalent or non-covalent interaction, thus improving the stability and reusability of biosensors (Table 5) [144–146].

Natural enzymes can catalyze the redox reaction of analytes through an electron transfer between the enzyme and electrode. As a type of electrode modifier for third-generation biosensors, MOFs for enzyme immobilization can not only accelerate the electron transfer but also increase the stability of enzyme molecules during storage and operation [147–153]. The immobilization strategies can be classified into five groups: physical adsorption, the embedding method, covalent binding, cross-linking, and electrochemical polymerization [154,155]. Various MOFs (e.g., Cu–MOFs, ZIF-8, AuNPs/ZIF-8, MIL-100(Fe)/PtNP, and so on) have been employed to fix glucose oxidase (GOx) and glucose dehydrogenase (GDH) for the detection of glucose [156–161]. In the composites, MOFs can act as a secondary biomimetic catalyst for the reduction of produced  $H_2O_2$ . For example, ZIF-8 MOFs have been employed to prepare enzyme-MOFs composites due to their mild synthesis conditions. Ma et al. used ZIF-8 as the matrix for immobilizing methylene green and GDH for the measurement of glucose [162]. The “single-step” co-precipitation in the biomimetic mineralization method was developed to entrap different enzymes into ZIF-8, including GOx, organophosphate-degrading enzyme A, and  $\alpha$ -chymotrypsin [157,158,163]. Recently, GOx and hemin were entrained in a 3D nanocage-based ZIF for the electrochemical detection of glucose via enhanced cascade biocatalysis (Figure 4A) [164]. The outer shell of ZIF prevented the leakage of enzymes, while the interior nanocage provided a second restriction to immobilize the enzymes and maintain their conformational freedom. In this biosensor, GOx catalyzed the oxidation of glucose by  $O_2$  to generate gluconic acid and  $H_2O_2$ , which was initiated by the oxidation of hemin. The design of enzyme/MOF-based electrochemical sensors for the detection of  $H_2O_2$  is a research hotspot, such as horseradish peroxidase (HRP)/ZIF-67/MWCNTs, HRP/PCN-333(Fe), HRP/ZIF-8/GO, and so on [165–168]. Gong et al. reported an  $H_2O_2$  sensor using a microperoxidase-11/PCN-333(Al) composite [169]. Zhang et al. used the mesoporous and microporous ZIF-8 to immobilize cytochrome c (Cyt c) via electrostatic interaction (Figure 4B) [170]. The adsorption capacity and enzymatic activity of Cyt c were increased when it was immobilized in the ZIF-8 MOFs. An electrode coated with Cyt c/ZIF-8 showed a high sensitivity for the detection of  $H_2O_2$  in real samples. Besides this, enzymes/MOFs (e.g., tyrosinase/Ni-Zn-MOFs and tyrosinase/Cu–MOFs) have also been used to construct electrochemical sensing platforms for the detection of pollutants in food and the environment, such as phenol and BPA [171–173]. For example, Ma et al. reported the electrochemical determination of BPA, based on multilayer tyrosinase/Cu–TCPP [174].

When the targets are captured by antibodies or aptamers immobilized on the MOFs-modified electrode, the electrochemical impedance would significantly increase, thus inducing a decrease in the voltammetric or amperometric signal, due to the block of mass diffusion of redox probes to the electrode's surface [175–177]. MOFs and their composites (e.g., magnetic  $Fe_3O_4$ @TMU-21, AuNPs/Zn/Ni–ZIF-8-800@graphene, and Al–MOFs) were used to develop immunosensors for the electrochemical detection of human epidermal growth factor receptor 2, monensin, vomitoxin, and salbutamol [178–180]. For example, Biswas et al. reported a label-free electrochemical immunosensor for the detection of carbohydrate antigen 125, based on Zr-trimesic acid MOF (MOF-808)/CNT [181]. The specific antigen-antibody interaction prevented the transfer of  $[Fe(CN)_6]^{4-/3-}$  to the electrode surface. Li et al. reported an electrochemical immunosensor for the detection of alpha-fetoprotein, using AuNPs/ZIF-8 as the support [182].

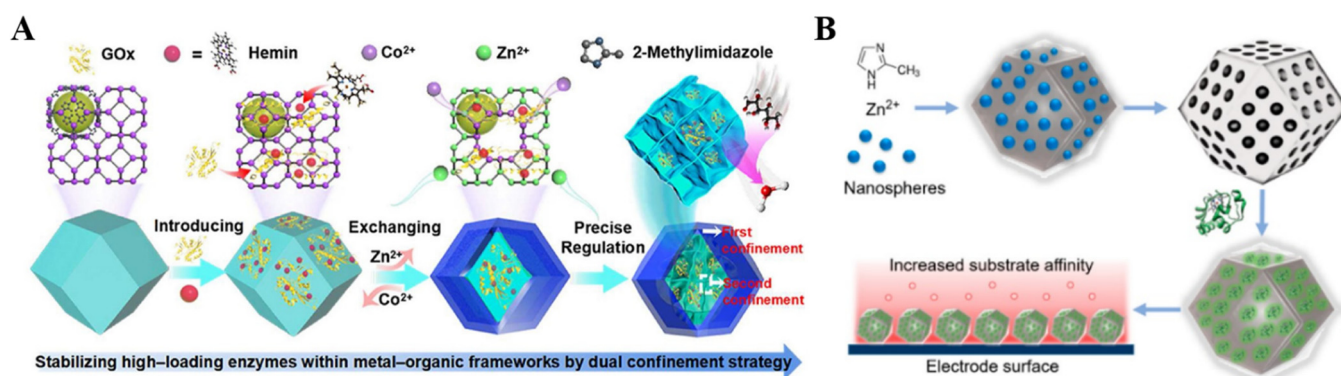


**Figure 4.** (A) Schematic illustration of the synthetic route of GOx/Hemin@NC-ZIF. Reprinted with permission from Ref. [164]. Copyright 2022, American Chemical Society. (B) Schematic illustration of the synthesis of Cyt c@mesoZIF-8 and the detection of  $\text{H}_2\text{O}_2$  with a Cyt c@mesoZIF-8/screen-printed electrode (SPE). Reprinted with permission from Ref. [170]. Copyright 2017, American Chemical Society.

DNA or RNA aptamers can be immobilized on MOFs via electrostatic interactions, hydrogen bonds,  $\pi$ - $\pi$  stacking, and van der Waal forces. Many aptamer/MOF-based electrochemical aptasensors have been developed for the determination of zearalenone, lysozyme, cocaine, CEA, and so on [183–186]. A CuMOF film electrode prepared using an electrodeposition method was used for the dual detection of *Staphylococcus aureus* [187]. As shown in Figure 5A, after the formation of a CuMOF film, AuNPs were electrodeposited on the film to load the DNA aptamers and enhance the electron transfer. When the micrococcal nucleases were secreted by the pathogen, aptamers were cleaved by the nuclease, and the ion movement was accelerated, resulting in an increase in the electrochemical signal of  $[\text{Fe}(\text{CN})_6]^{3-}/4-$ . Meanwhile, the pathogen captured by the aptamer led to a decrease in the electrochemical signal. To avoid the requirement of redox probes in the electrolyte, label-free, and redox probe-free biosensors can be developed by using electroactive MOFs as the substrates [188]. For example, Xing et al. reported a probe-free CuMOF-based electrochemical immunosensor for methyl jasmonate, in which numerous  $\text{Cu}^{2+}$  ions in the Cu-MOFs produced a strong redox signal directly [189].

Considering that DNA-based homogeneous electrochemical analysis allows target recognition in a homogeneous solution, it is important to develop a continuous homogeneous analysis system for rapid diagnosis and high-throughput bioanalysis. [190]. In homogeneous analysis, the working electrode usually has the ability to capture DNA, but its sensitivity is limited, due to the lack of signal amplification. Thus, Wang et al. developed a homogeneous electrochemical biosensor for the detection of miRNA using Co-MOF nanozyme-modified ITO electrodes (Figure 5B) [191]. The modified electrode could adsorb ssDNA via  $\pi$ - $\pi$  interactions and repel the MB-labeled hairpin DNA probe. The target miRNA could hybridize with the hairpin (HP) probe to form a DNA/miRNA strand. The DNA probe in the DNA/miRNA strand was cut by duplex-specific nuclease (DSN), then the released miRNA could hybridize with HP again, thus initiating the next cycle. The released MB-labeled short DNA strands were then adsorbed on the surface of MOF/ITO electrode. The MB tags could be electrochemically oxidized by the modified electrode in the presence of  $\text{H}_2\text{O}_2$ .

**Table 5.** Detection performances of different electrochemical sensors using MOFs as support platforms.

Type of MOFs	Analyte	Linear Range	LOD	Ref.
Ag@Zn–TSA	H <sub>2</sub> O <sub>2</sub>	0.3 μM~20000 μM	0.08 μM	[148]
ZIF-8@GOx	miRNA-21	0.1 nM~10 μM	29 pM	[149]
Cu–Hemin–GOx	Glucose	10~1555 μM	2.2 μM	[158]
PDA/ZIF-8@rGO	Glucose	1.2 μM~1.2 mM	0.333 μM	[159]
GDH/MG–Tb@MOF–CNTs	Glucose	25 μM~17 mM	8 μM	[161]
MG–ZIFs–GDH	Glucose	0.1~2 mM	Not reported	[162]
GOx/Hemin@NC–ZIF	Glucose	1~20 mM	10 μM	[164]
HRP/ZIF-67(Co)/MWCNT	H <sub>2</sub> O <sub>2</sub>	1.86~1050 μM	0.11 μM	[165]
HRP@PCN-333(Fe)	H <sub>2</sub> O <sub>2</sub>	0.5 μM~1.5 mM	0.09 μM	[166]
ZIFs@HRP/GO	H <sub>2</sub> O <sub>2</sub>	20 μM~6 mM	3.4 μM	[167]
MP-11-PCN-333(Al)–GO	H <sub>2</sub> O <sub>2</sub>	10~800 μM	3 μM	[168]
MP-11-PCN-333(Al)-3D-KSC	H <sub>2</sub> O <sub>2</sub>	0.387 μM~1.725 mM	0.127 μM	[169]
Cyt c@ZIF-8	H <sub>2</sub> O <sub>2</sub>	290 μM~3.6 mM	Not reported	[170]
Tyr@NiZn–MOF NSs	Phenol	0.08 μM~58.2 μM	6.5 nM	[171]
Tyr@Cu–MOFs	BPA	50 nM~3.0 μM	13 nM	[172]
Cu–BTABB–MOF@rGO	BPA	0~100 μM	0.208 μM	[173]
Tyr@Cu–TCPP	BPA	3.5 nM~18.9 μM	1.2 nM	[174]
AuPd NPs@UiO-66-NH <sub>2</sub> /CoSe <sub>2</sub>	Sulfaquinolaxine	1 pg/mL~100 ng/mL	0.547 pg/mL	[175]
Zn–MOF-on-Zr–MOF	PTK7	1 pg/mL~1.0 ng/mL	0.84 pg/mL	[177]
Fe <sub>3</sub> O <sub>4</sub> @TMU-21	HER2	1 pg/mL~100 ng/mL	0.3 pg/mL	[178]
MOF-808/CNTs	CA 125	0.001~0.1 and 0.1~30 ng/mL	0.5 pg/mL	[181]
AuNPs@ZIF-8	AFP	0.1 pg/mL~100 ng/mL	0.033 pg/mL	[182]
MTV polyMOF(Ti)	ZEN	10 fg/mL~10 ng/mL	8.9 fg/mL	[183]
493-MOF	Lysozyme	5 pg/mL~1 ng/mL	3.6 pg/mL	[184]
2D AuNCs@521–MOF	Cocaine	1 pg/mL~1 ng/mL	0.44 pg/mL	[185]
Cu–MOFs	<i>S. aureus</i>	7 – 7 × 10 <sup>6</sup> cfu/mL	1.9 cfu/mL	[187]
Cu–MOFs	HBsAg	1~500 ng/mL	730 pg/mL	[188]
Cu–MOF/COOH–GO	Methyl jasmonate	10 pM~100 μM	0.35 pM	[189]

**Abbreviation:** TSA, thiosalicylate; GOx, glucose oxidase; PDA, polydopamine; rGO, reduced graphene oxide; GDH, glucose dehydrogenases; MG, methylene green; CNTs, carbon nanotubes; HRP, horseradish peroxidase; MWCNT, multi-walled carbon nanotube; GO, graphene oxide; MP-11, microperoxidase-11; 3D-KSC, three-dimensional (3D) kenaf stem-derived porous carbon; Cyt c, cytochrome c; Tyr, tyrosinase; BPA, bisphenol A; TCPP, tetrakis(4-carboxyphenyl)porphyrin; PTK7, protein tyrosine kinase-7; HER2, human epidermal growth factor receptor 2; CA 125, carbohydrate antigen 125; AFP, alpha fetoprotein; MTV polyMOF(Ti), multivariate titanium metal–organic framework; ZEN, zearalenone; AuNCs, gold nanoclusters; CEA, carcinoembryonic antigen; *S. aureus*, *Staphylococcus aureus*; HBsAg, hepatitis B surface antigen; COOH-GO, carboxylated graphene oxide.

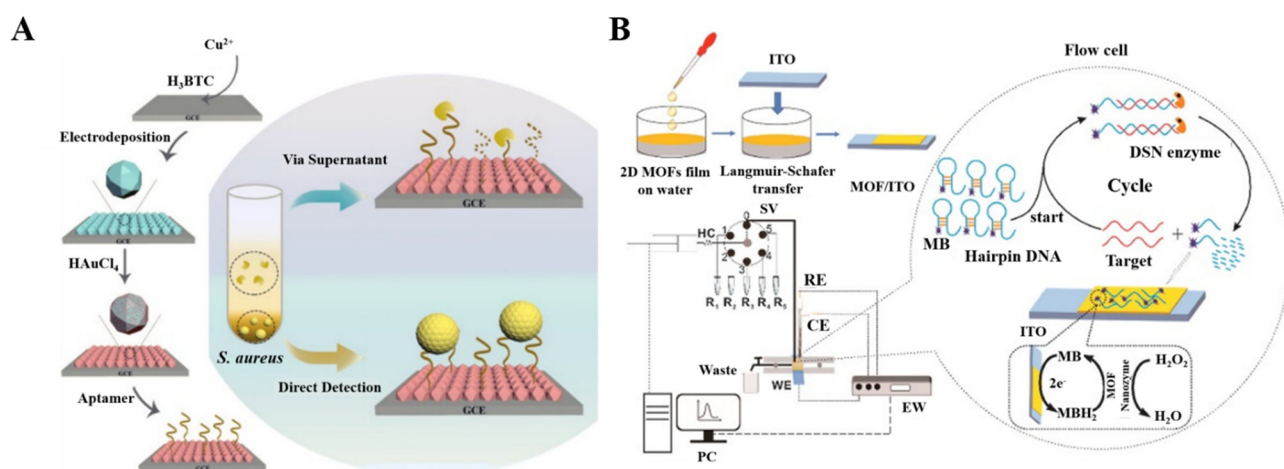


**Figure 5.** (A) Schematic illustration of the fabrication of the DNA/AuNPs/MOFs–based sensing platform and the electrochemical biosensor for the detection of *S. aureus* via supernatants and pathogen cells. Reprinted with permission from Ref. [187]. Copyright 2021, American Chemical Society. (B) Schematic illustration of the flow-homogeneous electrochemical assay system for microRNA based on MOF nanozyme. Reprinted with permission from Ref. [191]. Copyright 2022, Elsevier.

## 4. MOFs as Signal Labels

### 4.1. Nanocarriers

Because of their excellent properties, such as a large surface area, high porosity, good adsorption ability, and ease of functionalization, MOFs have been regarded as ideal matrices to load various functional materials for signal output and amplification, including electroactive small molecules, metal ions, enzymes, and nanoparticles (Table 6). Electroactive small molecules (e.g., ferrocene (Fc), 3,3',5,5'-tetramethylbenzidine (TMB), and MB) are always used as the labels of antibodies or nucleic acids for signal output. However, the weak electrochemical signal and the low marker number may limit the sensitivity of biosensors with electroactive small molecules as the labels. When many small molecules were loaded into MOFs, the signal would be greatly amplified, with the recognition element-labeled MOFs as the signal reporters [192,193]. For this purpose, electroactive molecule-encapsulated MOFs have been used as signal probes for the detection of the p53 gene, N<sup>6</sup>-methyladenine, procalcitonin, exosomes, and so on [194–197]. For example, the electroactive ferrocenecarboxylic acid was covalently confined in Zn–MOF as the signal tag for the detection of amyloid- $\beta$  [198]. Li et al. developed an immunosensor for C-reactive protein detection by loading toluidine blue in the channel of the Cu(II)–HKUST-1 [199]. Sun et al. reported an electrochemical biosensor for the detection of glioblastoma (GBM) –derived exosomes, with MB–loaded Zr–based UiO-66 MOFs as the signal reporters [200]. As displayed in Figure 6A, the peptide probes were modified on the electrode for the capture of exosomes by binding to human epidermal growth factor receptor (EGFR) and the EGFR variant (v) III mutation (EGFRvIII), overexpressed on the surface of exosomes. Then, the MB@UiO-66 probes were captured by the electrode, via the interaction between Zr<sup>4+</sup> ions in the MOFs and phosphate groups on the surface of exosomes. The method could quantify exosomes in the concentration range of  $9.5 \times 10^3 \sim 1.9 \times 10^7$  particles/ $\mu$ L by monitoring the signal change of MB.

The low signal-conversion efficiency based on the ratio of aptamer and target may severely limit the detection sensitivity. Through the DNA–based target cycling amplification, Zhang et al. developed a biosensor for enrofloxacin (ENR) detection by using thionine (Thi)–loaded AuNP-coated bimetallic MOF (Thi–Au@ZnNi–MOF) as the signal label (Figure 6B) [201]. In this study, the signal was amplified by the Pb<sup>2+</sup>-dependent DNAzyme-driven DNA walker. The hairpin DNA (HP1) and the hybrid of wDNA and the ENR aptamer (APT) were self-assembled on an electrode modified with Au&Pt–coated hollow cerium oxide (AuPt@h–CeO<sub>2</sub>) and polyethyleneimine (PEI)–functionalized molybdenum disulfide (PEI–MoS<sub>2</sub>). The APT was released from the electrode surface after binding to ENR. The resulting wDNA could cleave the HP1 in the presence of Pb<sup>2+</sup>, thus resulting in the formation of numerous capture probes. This allowed for the capture of Thi–Au@ZnNi–MOF through an interaction between the capture probe on the electrode and the signal probe on the Thi–Au@ZnNi–MOF. By monitoring the signal change with square wave voltammetry (SWV), ENR was determined with a linear range of  $5.0 \times 10^{-6}$  to  $1.0 \times 10^{-2}$  ng/mL.

MOFs (e.g., Cu–TCPP, UiO-66-NH<sub>2</sub>) could be employed to carry different signal molecules for the simultaneous detection of multiple targets, such as CEA and carbohydrate antigen 125 (CA125), KANA, and CAP [202,203]. For instance, Chang et al. reported a DNA–functionalized MOF–based homogeneous electrochemical biosensor for the simultaneous determination of multiple tumor biomarkers [204]. As shown in Figure 7A, two electroactive molecules (MB and TMB) were encapsulated into MOFs, and different double-stranded DNA (dsDNA) hybrids were used as the gatekeepers to cap the pore and prevent the release of the electroactive tags, respectively. In the presence of let-7a and miRNA-21, the corresponding dsDNA hybrids were unfolded through the toehold-mediated strand-displacement reaction. Then, the signal molecules were released and quantitatively measured by the electrode. The targets of let-7a and miRNA-21 were simultaneously determined, with an LOD down to 3.6 and 8.2 fM, respectively. Due to the well-defined SWV signals at different potentials, metal ions (e.g., Cd<sup>2+</sup>, Pb<sup>2+</sup>, Zn<sup>2+</sup>

and  $\text{Cu}^{2+}$ ) have been entrapped into MOFs as the signal labels for the simultaneous detection of different targets. For example, Yang et al. used UiO-66- $\text{NH}_2$  to load  $\text{Cd}^{2+}$  and  $\text{Pb}^{2+}$  ions for the detection of triazophos and thiachloprid [205]. UiO-66- $\text{NH}_2$  was used to carry many metal ions ( $\text{Pb}^{2+}$  and  $\text{Cd}^{2+}$ ) as the labels for the simultaneous detection of oxytetracycline and kanamycin [206]. Chen et al. proposed an electrochemical method for the simultaneous determination of multiple antibiotics using an amine-functionalized nanoscale MOF (NMOF) as the signal label (Figure 7B) [207]. In this work, the NMOF was modified with the complementary DNA of the kanamycin (KANA) aptamer (cDNA1) or chloramphenicol (CAP) aptamer (cDNA2). Then,  $\text{Pb}^{2+}$  and  $\text{Cd}^{2+}$  ions were loaded on the cDNA1-modified NMOF and cDNA2-modified NMOF, respectively. The two types of NMOFs could be captured by aptamer-modified magnetic beads. In the presence of KANA and CAP, the complementary DNA-modified NMOFs were released and were then determined by SWV under magnetic separation. The detection limits for KANA and CAP were 0.16 pM and 0.19 pM, respectively.

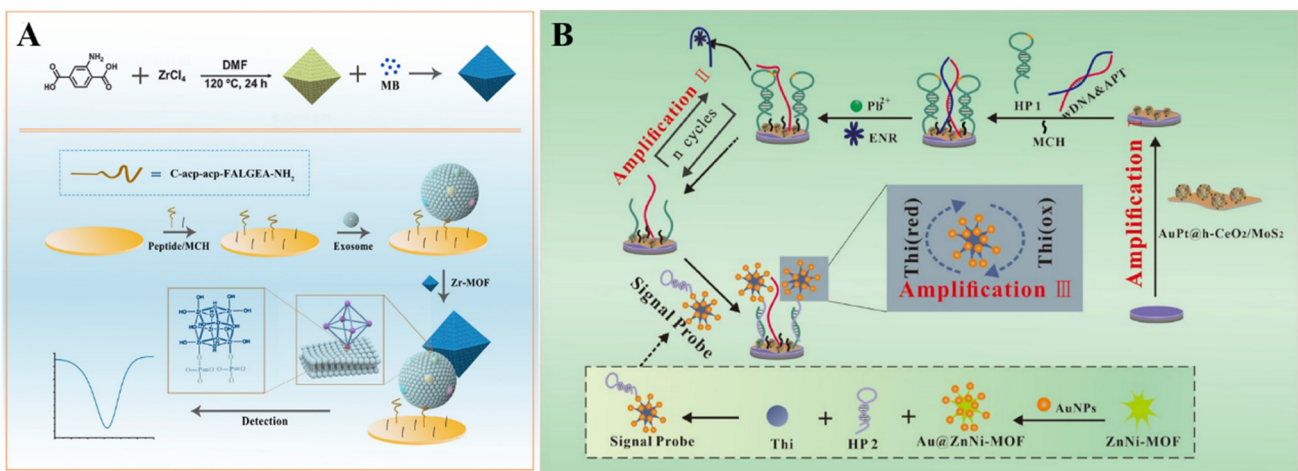


**Figure 6.** (A) Schematic illustration of the fabrication process of eMB@UiO-66-based nanoprobe and the principle of an electrochemical biosensor for the detection of GBM-derived exosomes. Reprinted with permission from Ref. [200]. Copyright 2021, American Chemical Society. (B) Schematic illustration of a Au@ZnNi-MOF-labeled electrochemical aptasensor for the detection of enrofloxacin. Reprinted with permission from Ref. [201]. Copyright 2022, Elsevier.

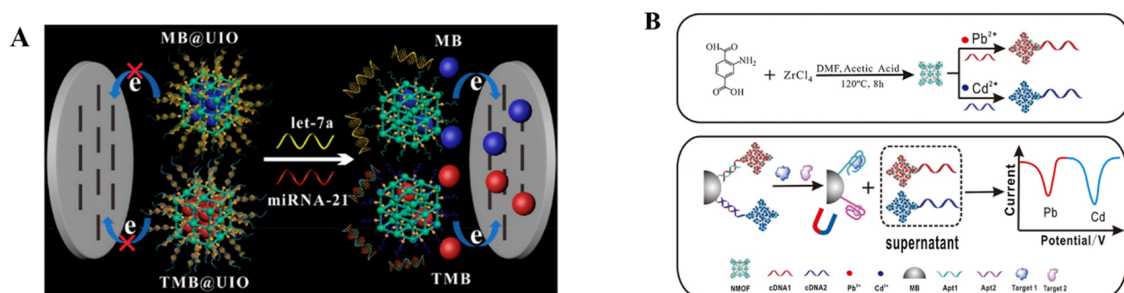


**Figure 7.** (A) Schematic illustration of the principle of a MOF-based homogeneous electrochemical biosensor for the multiple detection of miRNAs (let-7a and miRNA-21). Reprinted with permission from Ref. [204]. Copyright 2019, American Chemical Society. (B) Schematic illustration of the synthesis of UiO-66- $\text{NH}_2$  nanoparticles and preparation of two signal probes, and the simultaneous electrochemical detection of KANA and CAP, based on aptamer-nanoscale MOFs as biocodes. Reprinted with permission from Ref. [207]. Copyright 2017, Elsevier.

Hemin is a redox mediator with a reversible Fe(III)/Fe(II) redox pair and shows peroxidase-like catalytic activity [208]. However, the dimerization and oxidative decompo-

sition of hemin result in a finite catalytic lifetime. MOFs with high porosity can fix hemin to prevent dimerization and self-destruction. Meanwhile, hemin can endow MOFs with excellent enzyme-mimicking catalytic ability. For example, hemin/Fe-MIL-88 was used as the signal probe for the detection of fibroblast growth factor receptor 3 gene and thrombin [209]. Ling et al. employed Cu–MOFs (HKUST-1) to encapsulate redox-active FeTCPP and the recognition element of streptavidin (SA) for DNA detection (Figure 8) [210]. In the presence of target DNA, the hairpin DNA on the electrode surface was unfolded to form a structure with the combinative SA aptamer. Then, the FeTCPP@MOF–SA composites were immobilized on the electrode surface, based on the specific recognition between SA and its aptamer. The composites could catalyze the oxidation of ophenylenediamine (o-PD) to 2,2'-diaminoazobenzene, producing a high electrochemical signal. This “signal-on” aptasensor showed a wide linear range and an LOD down to 0.48 fM. To avoid the use of the unstable  $H_2O_2$  and redox mediate, Xie et al. developed an electrochemical aptasensor for thrombin (TB) detection with hemin-decorated MOFs [211]. Fe–MOFs- $NH_2$  was used to encapsulate hemin and AuNPs were used for the conjugation of aptamer and GOx. In the presence of TB, a large number of hemin molecules in Au/hemin@MOFs, captured by the electrode, acted as redox mediators to generate a strong electrochemical signal. The signal could be further amplified by the GOx–catalyzed generation of  $H_2O_2$ . Finally, the aptasensor exhibited a wide linear range (0.0001~30 nM) and a low LOD (0.068 pM) for TB detection.

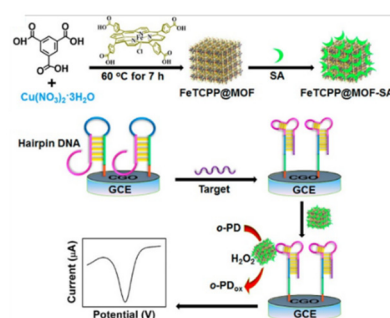


**Figure 8.** Schematic illustration of the synthesis of an FeTCPP@MOF–SA composite and electrochemical DNA sensing via the allosteric switch of hairpin DNA. Reprinted with permission from Ref. [210]. Copyright 2015, American Chemical Society.

MOFs, as enzyme nanocarriers, show high loading capacity. More importantly, MOFs can protect enzymes from biological, thermal, and chemical degradation and still maintain their biological activities. Therefore, enzyme/MOFs, such as GOx/ZIF-8, HRP/Au@Pt/MIL-53(Al), and HRP/Pt/PCN-224 have been used as the signal labels of biosensors to detect CA-242, the COVID-19 nucleocapsid protein, and breast cancer cells [212–214]. For instance, Liu et al. developed an electrochemical immunosensor for zearalenone (ZEN) detection, with HRP and IgG-encapsulated ZIFs (HRP/Ab@ZIF-L) as the signal tags (Figure 9A) [215]. The captured HRP/Ab@ZIF-L could catalyze the electrochemical oxidation of TMB in the presence of  $H_2O_2$ . Li et al. encapsulated GOx and HRP in ZIF-90 for the enzyme cascade reaction to amplify an electrochemical signal [216]. Alkaline phosphatase (ALP) can catalyze the hydrolysis of inert substrates into redox-active products. Recently, Feng et al. designed an electrochemical immunosensor, using Thi– and ALP–loaded ZIFs as the signal tags (Figure 9B) [217]. In this work, bovine serum albumin (BSA) was attached to the surface of ZIF-8 for the immobilization of antibodies and ALP through covalent interactions. ALP catalyzed the hydrolysis of p-aminophosphate ester (p-APP) to produce p-aminophenol (p-AP). The resulting p-AP led to the formation of AgNPs on the electrode surface by the reduction of  $Ag^+$  ions. Because of the excellent conductivity of AgNPs, an amplified electrochemical signal from the oxidation of Thi was observed. This method allowed for the detection of carbohydrate antigen 72–4 (CA 72–4), with a linear range of 1  $\mu$ U/mL–10 U/mL.

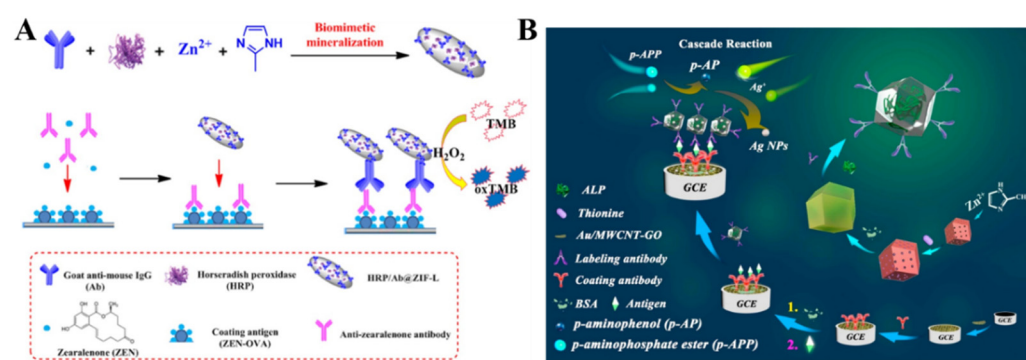


**Figure 9.** (A) Schematic illustration of the synthetic process for HRP/Ab@ZIF-L and the corresponding HRP/Ab@ZIF-L–based ELISA for the detection of ZEN. Reprinted with permission from Ref. [215]. Copyright 2021, Elsevier. (B) Schematic illustration of the construction steps and mechanism of a dual-labeling ZIF-8-based immunosensor for the electrochemical detection of tumor markers. Reprinted with permission from Ref. [217]. Copyright 2021, Elsevier.

The hybrid composites of MOFs and nanomaterials can be prepared via encapsulation or physical adsorption, which shows better performance than the single component in electrochemical analysis [218–221]. For example, Zhong et al. reported the detection of *Escherichia coli* O157:H7 (*E. coli* O157:H7) using CdS QDs–encapsulated ZIF-8 MOFs (CdS@ZIF-8) as the signal probes [222]. As shown in Figure 10A, *E. coli* O157:H7 was captured by the antibody and poly(*p*-aminobenzoic acid) (PABA)-modified electrode, which allowed for the attachment of the antibody-modified CdS@ZIF-8 probes. Then, a large number of Cd(II) ions were released by treating the electrode with HCl. The released Cd(II) ions were determined by differential pulse voltammetry (DPV). As a result, *E. coli* O157:H7 was detected, with a linear range of 10~10<sup>8</sup> CFU/mL and an LOD of 3 CFU/mL. However, dissolution by strong acids or oxidants and pre-concentration before electrochemical measurement is complicated and time-consuming. To simplify the experimental procedures, Wang et al. reported the detection of telomerase, using SA–covered AgNP–loaded PCN-224 MOFs (SA–AgNPs/PCN-224) as the signal reporter (Figure 10B) [223]. The elongation of a primer by telomerase led to the formation of an SA aptamer, due to the allosteric activation hairpin probe on the electrode surface. Then, the SA–AgNPs/PCN-224 probe was captured by the electrode through SA–aptamer interaction. A strong electrochemical signal was observed due to the highly characteristic solid-state Ag/AgCl process of AgNPs in the KCl electrolyte medium. The telomerase concentration could be determined by monitoring the signal change from AgNPs.

Metal, bimetallic alloy, and metal oxide nanoparticles are of great significance in electrocatalysis and electrochemical bioassays, due to their excellent electrocatalytic activity and relatively high stability. They have been integrated with MOFs to exhibit higher catalytic efficiency and enhance detection sensitivity, due to the synergistic effect [224]. Electrochemical biosensors based on the composites of MOFs and metal nanoparticles (e.g., hemin–MOFs/PtNPs, AgPt/PCN-223-Fe, and Pd/MIL101-NH<sub>2</sub>) have been developed for the detection of FGFR3 gene mutation, ochratoxin A, telomerase activity, and so on [209,213,225–229]. For instance, Ling et al. synthesized the composites of PtNPs and UiO-66-NH<sub>2</sub> MOFs via a one-step method and then used them to determine the telomerase activity [230]. Yu et al. developed a Pb<sup>2+</sup> sensor by using Pd/Pt–modified Fe–MOFs (Fe–MOFs/PdPt) as the signal reporters [231]. As displayed in Figure 11, the substrate DNA strands attached to the rGO–tetraethylene pentamine-gold nanoparticle (rGO-TEPA-Au)-modified electrode were enzymatically cleaved in the presence of Pb<sup>2+</sup>, which led to the formation of short-signal DNA strands. Then, the hairpin DNA-modified Fe–MOFs/PdPt probes were captured by binding them with the signal DNA strands to catalyze the electrochemical reaction of H<sub>2</sub>O<sub>2</sub>.

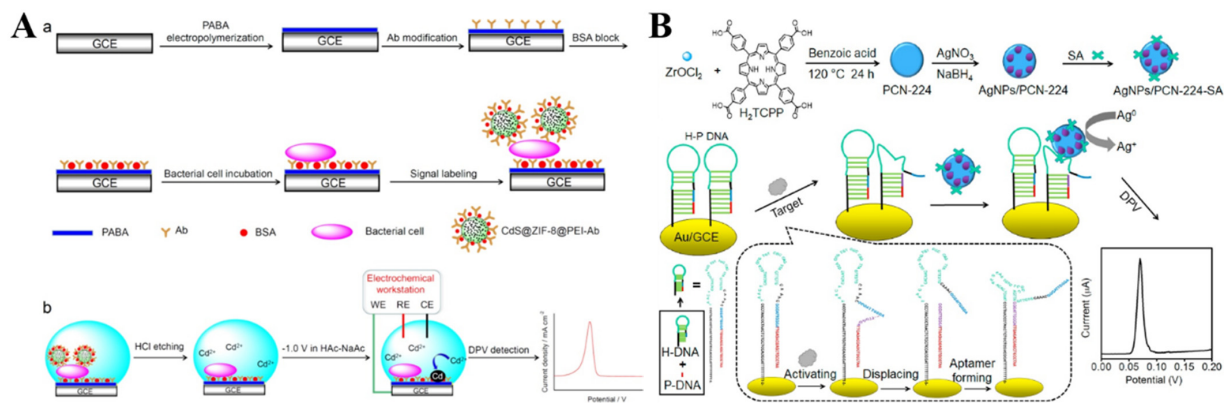


**Figure 10.** (A) Schematic illustration of (a) the fabrication steps of the sandwich-type electrochemical immunobiosensor for the detection of *E. coli* O157:H7 using CdS@ZIF-8 as signal tags. (b) Schematic illustration of the steps for DPV detection. Reprinted with permission from Ref. [222]. Copyright 2019, Elsevier. (B) Schematic illustration of the construction of an SA-modified AgNPs/PCN-224 probe and a direct electrochemical sensing strategy of telomerase activity via a conformation switch from aptamer-closed hairpin DNA to aptamer-on hairpin DNA. Reprinted with permission from Ref. [223]. Copyright 2021, Elsevier.

**Table 6.** Detection performances of different electrochemical sensors, using MOFs as nanocarriers.

Type of MOFs	Analyte	Linear Range	LOD	Ref.
Zn-MOF/Fe <sub>3</sub> O <sub>4</sub> -COOH/Thi	CTnI	0.04~50 ng/mL	0.9 pg/mL	[192]
MB@Zr-MOFs	patulin	50 fg/mL~5 $\mu\text{g/mL}$	14.6 fg/mL	[193]
MB@MIL-101-NH <sub>2</sub> (Cr)	p53 gene	10 fM~100 nM	1.4 fM	[194]
MB@Zr-MOFs	N <sup>6</sup> -methyladenine	1 fM~1 nM	0.89 fM	[195]
UiO-66-TB	procalcitonin	1 pg/mL~100 ng/mL	0.3 pg/mL	[196]
GDH@ZIF-8/[Fe(CN) <sub>6</sub> ] <sup>3-</sup> /UiO-66	exosome	$1.0 \times 10^3$ ~ $1.0 \times 10^8$ particles/mL	300 particles/mL	[197]
Fc-Zn-MOF	amyloid- $\beta$	0.1 pg/mL~100 ng/mL	0.03 pg/mL	[198]
Cu-MOFs-TB	CRP	0.5~200 ng/mL	166.7 pg/mL	[199]
MB@Zr-MOFs	exosome	$9.5 \times 10^3$ ~ $1.9 \times 10^7$ particles/ $\mu\text{L}$	$7.83 \times 10^3$ particles/ $\mu\text{L}$	[200]
Au@ZnNi-MOF	enrofloxacin	5 fg/mL~10 pg/mL	0.102 fg/mL	[201]
Cu-TCPP-TB and PB	CEA and CA125	0.1~160 ng/mL and 0.5~200 U/mL	0.03 ng/mL and 0.05 U/mL	[202]
HP-UiO-66-MB and Fc	KANA and CAP	0.1 pM~50 nM	35 fM and 21 fM	[203]
UiO-66-NH <sub>2</sub> -MB and TMB	let-7a and miRNA-21	0.01~10 and 0.02~10 pM	3.6 fM and 8.2 fM	[204]
UiO-66-NH <sub>2</sub> -Cd <sup>2+</sup> and Pb <sup>2+</sup>	TRS and THD	0.2~750 ng/mL	0.07 and 0.1 ng/mL	[205]
hemin-MOFs/PtNPs	FGFR3 gene mutation	0.1 fM~1 nM	0.033 fM	[209]
FeTCPP@MOF-SA	DNA	10 fM~10 nM	0.48 fM	[210]
MB-GOx-ZIF-8/Au-rGO	CA 242	0.001~1000 U/mL	69.34 $\mu\text{U/mL}$	[212]
HRP/hemin/G-quadruplex Au@Pt/MIL-53 (Al)	nucleocapsid protein	0.025~50 ng/mL	8.33 pg/mL	[213]
HRP/hemin/Gquadruplex PtNPs/PCN-224	Cancer cells	20~ $1 \times 10^7$ cells/mL	6 cells/mL	[214]
HRP/Ab@ZIF-L	ZEN	0.5 ng/L~0.476 $\mu\text{g/L}$	0.5 ng/L	[215]
GOx/HRP/ZIF-90	CA-125	0.1 pg/L~40 $\mu\text{g/L}$	0.05 pg/mL	[216]
CdS@ZIF-8	<i>Escherichia coli</i> O157:H7	$10 \sim 10^8$ CFU/mL	3 CFU/mL	[222]
AgNPs/PCN-224	telomerase activity	$1 \times 10^{-7}$ ~ $1 \times 10^{-1}$ IU/L	$5.4 \times 10^{-8}$ IU/L	[223]
Cu <sub>2</sub> O@Cu-MOF@AuNPs	CEA	50 fg/mL~80 ng/mL	17 fg/mL	[224]
AgPt/PCN-223-Fe	ochratoxin A	20 fg/mL~2 ng/mL	14 fg/mL	[225]
Pd/MIL101-NH <sub>2</sub>	telomerase activity	$5 \times 10^2$ ~ $1.62 \times 10^7$ HeLa cells/mL	11.25 HeLa cells/mL	[226]
Pd@UiO-66	miRNA-21	20 fM~600 pM	0.713 fM	[227]
PdNPs@Fe-MOFs	miRNA-122	0.01 fM~10 pM	0.003 fM	[228]
Pd@PCN-222	ochratoxin A	10 fg/mL~10 ng/mL	6.79 fg/mL	[229]
Pt@UiO-66-NH <sub>2</sub>	telomerase activity	$5 \times 10^2$ ~ $1 \times 10^7$ HeLa cells/mL	$2.0 \times 10^{-11}$ IU/L	[230]
Fe-MOFs/PdPt NPs	Pb <sup>2+</sup>	5 pM~1 $\mu\text{M}$	2 pM	[231]

**Abbreviation:** Thi, thionine; CTnI, cardiac troponin-I; MB, methylene blue; TB, toluidine blue; GDH, glucose dehydrogenase; Fc, ferrocene; CRP, C-reactive protein; TCPP, tetrakis(4-carboxyphenyl)porphyrin; PB, Prussian blue; CEA, carcinoembryonic antigen; CA125, carbohydrate antigen 125; KANA, kanamycin; CAP, chloramphenicol; TMB, 3,3',5,5'-Tetramethylbenzidine; TRS, triazophos; THD, thioclopid; SA, streptavidin; GOx, glucose oxidase; rGO, reduced graphene oxide; HRP, horseradish peroxidase; ZEN, zearalenone.

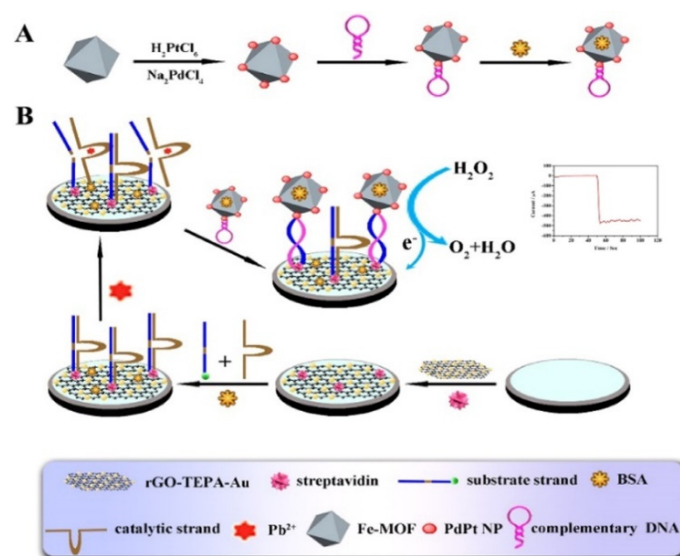


**Figure 11.** Schematic diagram of: (A) the preparation process of Fe–MOFs/PdPt NPs–HP, and (B) schematic representation of the proposed strategy for the biosensor. Reprinted with permission from Ref. [231]. Copyright 2018, Elsevier.

#### 4.2. Electroactive Labels

The elaborate selection of metal ions and organic ligands can endow MOFs with unique functionality, including optical and electrochemical properties and catalytic activity. MOFs with redox-active metal ions or ligands as the precursors can be directly utilized as the electrochemical signal labels of biosensors without acid dissolution (Table 7). Taking advantage of their specific voltammetric signals at different potentials, MOFs with redox-active metal ions (e.g., Cu–MOFs, Cd–MOFs, and Co–MOFs) are used as the electroactive probes for the detection of endotoxin, CEA, thrombin, prostate-specific antigen, microRNA, and so on [232–240]. Liu et al. reported an electrochemical immunosensor for the detection of C-reactive protein by using Cu–MOFs as signal probes [241]. In this study, AuNPs were used to decorate Cu–MOFs with improving conductivity, and PtNP–modified covalent organic frameworks were utilized as the electrode substrates. After the formation of sandwich-like immuno-complexes, the MOFs composites with a large amount of  $\text{Cu}^{2+}$  ions produced a high electrochemical signal. The immunosensor showed a wide linear range (1–400 ng/mL) for C-reactive protein detection. Recently, Dong et al. reported an aptasensor for  $\text{Pb}^{2+}$  detection, with PtNPs@Cu–MOF as the signal reporter (Figure 12A) [242]. In this work, DNA walker signal amplification was used to improve the sensitivity through the recognition of an rA site in the DNA walker-substrate strand (SS). In the presence of  $\text{Pb}^{2+}$ , the SS mixture on the electrode surface could be split, thus producing two single S1 and S2 chains. After DNA walker signal amplification, the hairpin DNA–modified PtNPs@Cu–MOF nanocomposites were captured by an electrode covered with the residual DNA fragments. The  $\text{Pb}^{2+}$  concentration was determined by the current change from Cu–MOF.

To meet the requirements of the point-of-care (POC) test applications, Chen et al. reported a dual-response biosensor for the electrochemical and glucometer detection of DNA methyltransferase activity, based on invertase–modified Cu–MOFs [243]. As shown in Figure 12B, the Cu–MOFs were sequentially modified with AuNPs, capture probes (CP), and invertase (invertase/CP/Au/CuMOFs). The Au/CuMOFs hybrid composites served as electroactive probes for the production of electrochemical signals and as the support matrixes for the immobilization of invertase. In the presence of Dam MTase, the hairpin probe 1 (HP1) was methylated and then hydrolyzed with the assistance of restriction endonuclease (DpnI). The released binding sequence opened the hairpin probe 2 (HP2) that was immobilized on the electrode surface via hybridization. The exposed

sticky terminus on the electrode surface was then hybridized with the CP to tether the invertase/CP/Au/CuMOFs. The electrochemical response of  $\text{Cu}^{2+}$  ions in Cu–MOFs was recorded by DPV. Invertase in the conjugate catalyzed the hydrolysis of sucrose to generate glucose, which could be readily detected using a personal glucometer.

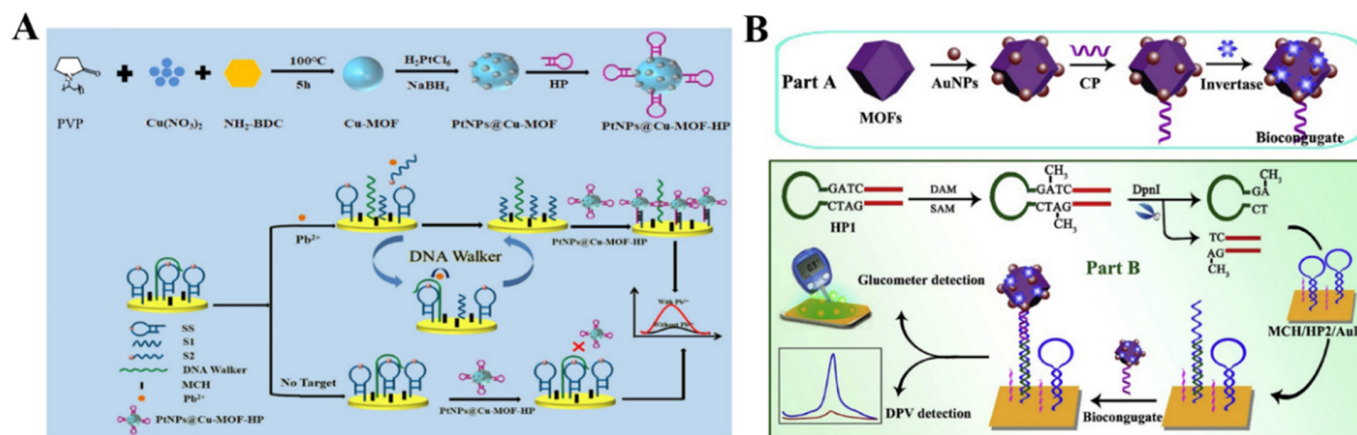


**Figure 12.** (A) Schematic illustration of the fabrication of PtNPs@Cu–MOF–HP/ $\text{Pb}^{2+}$ /MCH/DNA walker-SS/AuE sensor and the mechanism of  $\text{Pb}^{2+}$  detection. Reprinted with permission from Ref. [242]. Copyright 2022, Elsevier. (B) Schematic illustration of the stepwise preparation of invertase/CP/Au/CuMOF bioconjugates and the fabrication process of this proposed dual-response biosensor for Dam MTase activity assay. Reprinted with permission from Ref. [243]. Copyright 2019, Elsevier.

MOFs with  $\text{NH}_2\text{-BDC}$  as the ligand can be directly used as electroactive signal reporters, which is attributed to the oxidation of amino groups in the ligands [244]. For this view, Li et al. developed an electrochemical biosensor by integration of magnetic separation with nuclease-assisted walking DNA nanomachine [245]. As shown in Figure 13A, the hybrid formed between the MUC1 aptamer and blocker DNA probe (BDP) was immobilized on the surface of a magnetic bead. In the presence of the MUC1 protein, the BDP was released from the surface of the magnetic bead, thus opening the hairpin DNA attached to the AuNPs/MXene–modified electrode. With exonuclease III (Exo III)-assisted cycle amplification, the 3'-end part of DNA in the BDP/DNA hybrid was cut, and the released BDP was moved on the electrode surface to trigger other enzymatic reactions. The residual DNA fragments on the electrode could hybridize with the hairpin DNA probes attached to the AuNPs/UiO-66- $\text{NH}_2$  MOFs, thus producing an enhanced DPV signal from the oxidation of 2-ATPA ligands in the MOFs. Recently, Dong et al. reported a ratiometric dual-signal electrochemical biosensor for the detection of miRNA, based on Fe–MOFs and UiO-66- $\text{NH}_2$  [246]. As displayed in Figure 13B, the Fe–MOFs- $\text{NH}_2$  composites were functionalized, with hairpin H2 probes as the signal tags. The MB-GA-UiO-66- $\text{NH}_2$  composites were used to modify the electrode for the electrodeposition of AuNPs to immobilize the captured hairpin H1 probes. In the presence of target miRNA-155, the catalytic hairpin assembly (CHA) reaction was triggered, and numerous Fe–MOFs were tethered on the electrode, generating an increased electrochemical signal. Meanwhile, the nanoprobe with poor conductivity hindered the electron transfer, leading to a decrease in the DPV response from MB. The target concentration was determined by monitoring the change in the ratio response of  $I_{\text{Fe-MOFs}}/I_{\text{MB}}$  with a LOD of 50 aM. A ratiometric biosensor with an electroactive species acting as the inner reference probe can improve detection accuracy. Xie et al. reported a sandwich ratiometric electrochemical aptasensor by using Fe–MOF (Fe–MIL-88) and  $[\text{Fe}(\text{CN})_6]^{3-/4-}$  as the signal reporter and inner reference probe, respectively [247]. A three-dimensional DNA-nanotetrahedron that can eliminate non-specific adsorption from biomolecules was immobilized on the surface of an AuNPs@IL-MoS<sub>2</sub> electrode for the capture of a target (TB). The signal DNA–modified Au NPs@Fe-MIL-88

could be attached to the electrode surface by binding with the captured target, thus producing an oxidation peak at 0.8 V. With the increase in target concentration, the current from the signal reporter increased, while there was no significant change in the peak current of the inner reference probe. The target concentration was determined according to the ratio response of  $I_{\text{signal reporter}}/I_{\text{inner reference}}$ , with a LOD down to 59.6 fM.

**Table 7.** Detection performances of different electrochemical sensors by using MOFs as electroactive labels.

Type of MOFs	Analyte	Linear Range	LOD	Ref.
Cu–BTC MOFs	lipopolysaccharide	1.0 pg/mL~1.0 ng/mL	0.29 pg/mL	[232]
Ag–MOFs	CEA	0.05~120 ng/mL	8 fg/mL	[233]
PtPd NPs/Co–MOFs	thrombin	1 pM~30 nM	0.32 pM	[234]
AuNPs/Cu–MOFs	miRNA-155	1.0 fM~10 nM	0.35 fM	[235]
ZIF-67/ZIF-8	PSA	5 pg/mL~50 ng/mL	0.78 pg/mL	[236]
Cd–MOFs	ochratoxin A	0.05~100 ng/mL	10 pg/mL	[237]
Cd–MOFs-74	p53 gene	0.01~30 pM	6.3 fM	[238]
Cu–MOFs@PtPd NPs	Hg <sup>2+</sup>	0.001~100 nM	0.52 pM	[239]
Co–MOFs@AuNPs	Mucin 1	0.004~400 pM	1.34 fM	[240]
Cu–MOFs@AuNPs	CRP	1~400 ng/mL	0.2 ng/mL	[241]
PtNPs@Cu–MOF	Pb <sup>2+</sup>	3.0 pM~5 μM	0.2 pM	[242]
Invertase/Cu–MOF	DNA methyltransferase activity	0.002~1 U/mL	0.001 U/mL	[243]
MIL-101(Fe)	telomerase activity	$1 \times 10^{-6} \sim 5 \times 10^{-2}$ IU/L	$1.8 \times 10^{-7}$ IU/L	[244]
UiO-66-NH <sub>2</sub>	Mucin 1	5 pg/mL~ 50 ng/mL	0.72 pg/mL	[245]
Fe–MOFs/MB–GA–UiO-66-NH <sub>2</sub>	miRNA	1 fM~100 nM	50 aM	[246]
Fe–MOFs@AuNPs	thrombin	0.298~29.8 pM	59.6 fM	[247]

**Abbreviation:** BTC, 1,3,5-benzenetricarboxylic acid; CEA, carcinoembryonic antigen; AuNP, gold nanoparticles; PSA, prostate-specific antigen; CRP, C-reactive protein; MB, methylene blue; GA, graphene aerogel.

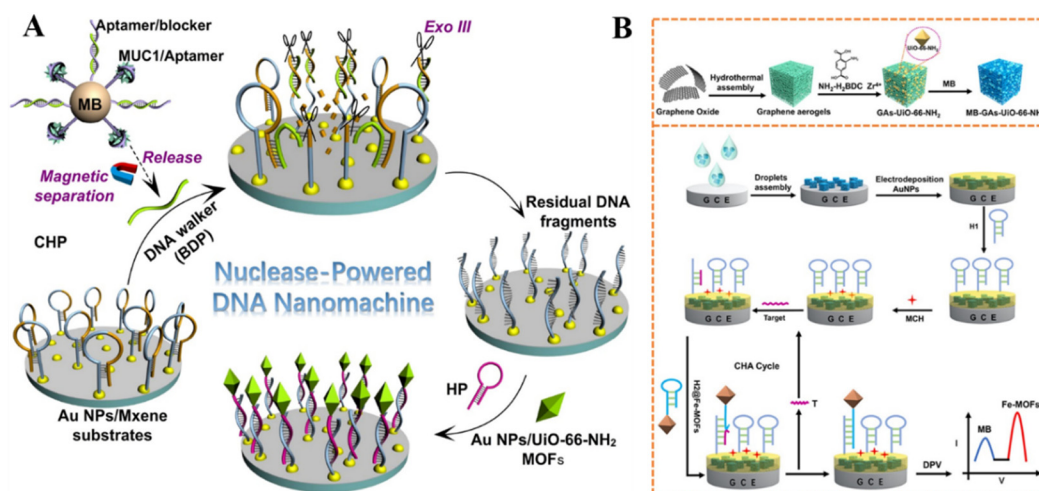


**Figure 13.** (A) Schematic illustration of AuNPs/UiO-66-NH<sub>2</sub> MOFs-based biosensor for protein biomarkers (MUC1) analysis with the DNA nanomachines powered by Exo III with cycle signal amplification. Reprinted with permission from Ref. [245]. Copyright 2022, Elsevier. (B) Schematic illustration of the MB–GA–UiO-66-NH<sub>2</sub> synthesis procedure and the principle of a ratiometric electrochemical biosensor for the detection of miRNA-155. Reprinted with permission from Ref. [246]. Copyright 2022, American Chemical Society.

#### 4.3. Electrocatalysts

Several types of MOFs have been documented to possess enzyme-mimicking catalytic activity, such as Ce–MOFs, Cu–MOFs, and Fe–MOFs, which are denoted as nanozymes. Compared with natural enzymes, these nanozymes have comparable catalytic perfor-

mances. More importantly, they can remain stable in different, harsh, conditions. Thus, the MOF nanozymes (e.g., Ce–MOFs and Cu–MOFs) have been used to develop electrochemical biosensors for the determination of bacterial lipopolysaccharide, hantavirus, carbohydrate antigen 15–3, and so on (Table 8) [248–251]. For example, Ce–MOFs can be used as electrocatalysts to design electrochemical biosensors in view of the redox property of  $\text{Ce}^{3+}/\text{Ce}^{4+}$ . Shen et al. developed an electrochemical aptasensor for lipopolysaccharide detection by using Ce–MOFs and  $\text{Zn}^{2+}$ –dependent DNAzyme-assisted recycling for dual signal amplification [252]. As illustrated in Figure 14A, the CeMOFs were decorated with AuNPs and the thiolated HP2 (HP2/AuNPs/CeMOFs). The presence of lipopolysaccharides triggered the release of the reporter DNA from the duplex. The released reporter DNA as a DNAzyme promoted the circular cleavage of HP1 probes. Then, the HP2/AuNPs/CeMOFs were recruited on the electrode to catalyze the electrochemical oxidation of AA. In addition, the CeMOFs were employed by Yu and co-workers to catalyze the oxidation of Thi for the detection of thrombin [253]. Dong et al. developed a ratiometric CeMOFs-based electrochemical biosensor for the detection of telomerase activity [254]. In this study, the MB–modified hairpin probe was hybridized with telomerase primer (TP) and then anchored to the electrode surface. After the telomerase-catalyzed extension, the hairpin probe was unfolded and the MB tag was farther away from the electrode surface, resulting in a decreased signal. Meanwhile, the CeMOFs/AuNPs catalyzed the oxidation of hydroquinone, leading to a “signal-on” electrochemical response.

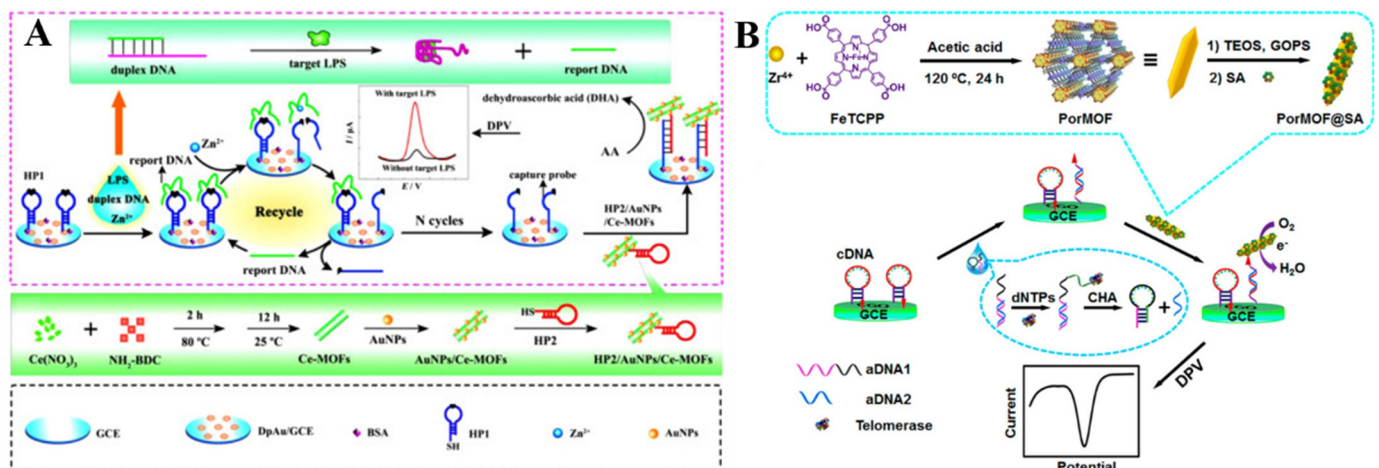


**Figure 14.** (A) Schematic illustration of the signal amplification strategy, the mechanism of LPS detection, and the preparation procedure of HP2/AuNPs/Ce–MOFs. Reprinted with permission from Ref. [252]. Copyright 2016, Elsevier. (B) Schematic illustration of the preparation of nanoscaled PorMOF and the electrochemical detection of telomerase activity via a telomerase-triggered conformation switch. Reprinted with permission from Ref. [255]. Copyright 2016, American Chemical Society.

Because of their peroxidase-like catalytic ability, porphyrinic MOFs (PCN-222 and (Fe-P)n-MOF) can be utilized as novel electrocatalysts for the analysis of DNA, T4 polynucleotide kinase, and prostate-specific antigen (PSA) [256–259]. Ling et al. reported a nanoscaled porphyrinic MOF (PorMOF)–based electrochemical biosensor for the detection of telomerase [255]. As shown in Figure 14B, the SA–modified PorMOF was synthesized, with iron porphyrin as the linker and  $\text{Zr}^{4+}$  ion as the node. In the presence of telomerase, the assistant DNA 1 (aDNA1) was catalytically extended to self-fold into a hairpin structure and the released assistant DNA2 (aDNA2) opened the cDNA through hybridization. Then, the PorMOF@SA nanoprobe was immobilized on the electrode surface through the biotin–SA interaction, which generated an enhanced signal via the electrocatalytic reduction of  $\text{O}_2$ . Cui et al. reported the electrochemical detection of  $\text{Pb}^{2+}$  with PorMOF decorated with AuNPs and  $\text{Pb}^{2+}$ –dependent DNAzyme [260]. In this work, the PorMOF/AuNPs

catalyzed the electrochemical oxidation of TMB by  $H_2O_2$ , greatly amplifying the current intensity.

**Table 8.** Detection performances of different electrochemical sensors by using MOFs as electrocatalysts.

Type of MOFs	Analytes	Linear Ranges	LOD	Ref.
$Cu^{2+}$ -NMOFs	lipopolysaccharide	0.0015~750 ng/mL	0.61 pg/mL	[248]
CuMOF	hantavirus	1 fM~1 nM	0.74 fM	[249]
Cu-MOFs@GOx	CA15-3	10 $\mu$ U/mL~10 mU/mL	5.06 $\mu$ U/mL	[250]
$pSC_4$ -AuNPs/Cu-MOFs	Fractalkine	10 pg/mL~10 $\mu$ g/mL	7.4 pg/mL	[251]
AuNPs/Ce-MOFs	lipopolysaccharide	10 fg/mL~100 ng/mL	3.3 fg/mL	[252]
Thi/AuNPs/Ce(III, IV)-MOF	thrombin	0.1 fM~10 nM	0.06 fM	[253]
AuNPs/Ce-MOF	telomerase activity	$2 \times 10^2$ ~ $2 \times 10^6$ cells/mL	27 cells/mL	[254]
PorMOF@SA	telomerase activity	$1 \times 10^2$ ~ $1 \times 10^7$ cells/mL	30 cells/mL	[255]
PCN-222@SA	DNA	10 fM~100 nM	0.29 fM	[256]
L/(Fe-P)n-MOF	T4 polynucleotide kinase	1.0 mU/mL~1.0 U/mL	0.62 mU/mL	[257]
GR-5/(Fe-P)n-MOF	$Pb^{2+}$	0.05~200 nM	0.034 nM	[260]

**Abbreviation:** GOx, glucose oxidase; CA15-3, carbohydrate antigen 15-3;  $pSC_4$ -AuNPs, para-sulfonatocalix [4] arene-coated gold nanoparticles; Thi, thionine; SA, streptavidin.

#### 4.4. Sacrificial Templates

Prussian blue (PB), a mixture of ferric and ferrous cyanide, has been widely used in the fields of biomedicine and electrochemistry. It can be used as a redox and electrocatalytic label for bioassays. However, its low stability in water limits the usage of PB in bioassays. Recently, porous Fe-MOFs have been used as metal precursors to produce electroactive PB NPs in situ for signal output and amplification. For example, Bao et al. reported a sensing platform for the detection of miRNA-21, based on the electrochemical conversion of Fe-MOFs into PB NPs [261]. As shown in Figure 15A–C, multipedal polydopamine nanoparticles-DNA (PDANs-DNA) nanomachines were designed that worked on the electrode via multiple legs under exonuclease III-driving. After the formation of DNA dendrimers through the assembly of two hairpins, the Fe-MIL-88-NH<sub>2</sub> MOFs were immobilized on the electrode. Under a high potential, an acid microenvironment was produced due to the generation of H<sup>+</sup> on the electrode surface via the water-splitting reaction [262], which made the release of Fe<sup>3+</sup> ions from MOFs. The released Fe<sup>3+</sup> ions were then electrochemically transformed into Prussian white (PW) in the presence of Fe(CN)<sub>6</sub><sup>3-</sup>. The PW was oxidized into PB by O<sub>2</sub> in the environment. The biosensor could determine miRNA-21 in the concentration range of 10 aM~10 pM with a LOD of 5.8 aM. Based on the conversion of Fe-MOFs into PB NPs in the presence of Fe(CN)<sub>6</sub><sup>3-</sup>, other biomarkers, such as non-small cell lung cancer ctDNA, T4 polynucleotide kinase, and miRNA-21 have been sensitively detected [263–265].

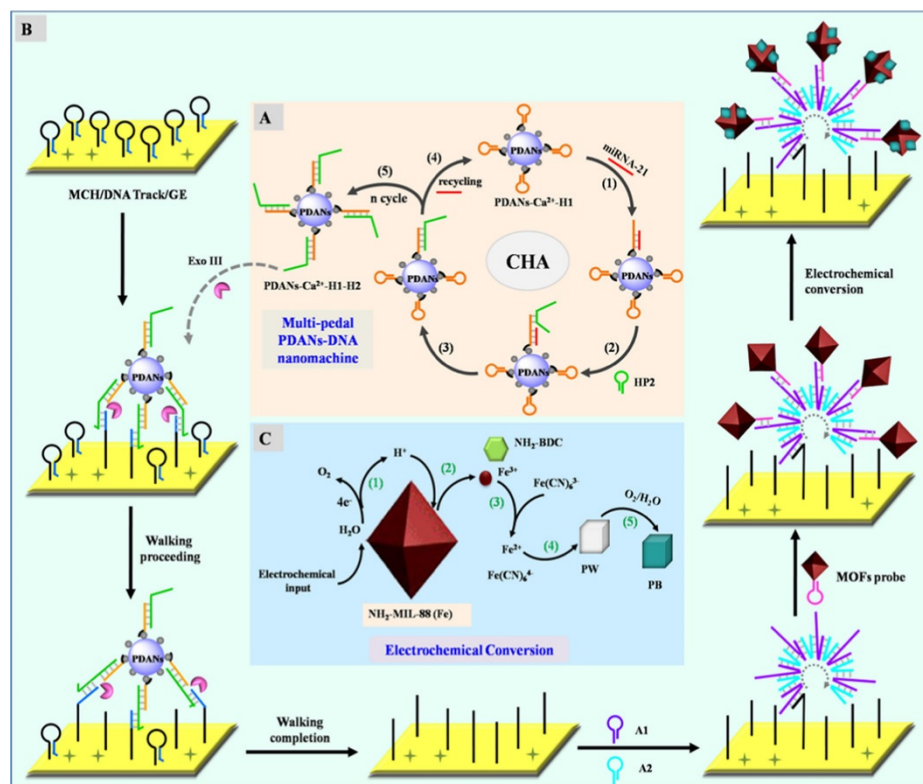


**Figure 15.** Schematic illustration of the biosensor of miRNA-21 based on PDANs–DNA nanomachine and the electrochemical conversion of MOFs. Reprinted with permission from Ref. [261]. Copyright 2021, American Chemical Society.

## 5. Conclusions and Future Aspects

In summary, MOF-based nanomaterials have shown outstanding performances in the development of electrochemical sensors. In this review, we comprehensively summarized the different roles of MOFs in the applications of electrochemical sensors. The intrinsic advantages that they offer have promoted the practicability of electrochemical sensors, including large surface area, high porosity, chemical functionality, tunable channel structure, and so on. To overcome the disadvantages of MOF-based nanomaterials (e.g., low conductivity and weak stability), multifunctional conductive materials have been integrated with MOFs to improve the performances of sensors by synergistic effects. Besides, various effective signal amplification strategies have been perfectly integrated into MOF-based electrochemical sensors, such as enzyme catalysis, DNA-based nanomachines, and functional nanomaterials.

Although extensive efforts are being made to improve the performance of MOF-based sensors, certain issues should be further researched to realize the full potential of MOFs. First, the utilization efficiency of electroactive or electrocatalytic metal ions in MOFs should be improved. In recent years, the quasi-MOFs prepared by the controlled deligandation of MOFs and the single-atom catalysts derived from MOFs have attracted extensive attention in different fields. Second, the size of MOFs has an important influence on their activity and stability; however, it is difficult to effectively adjust the size and shape of MOFs, which is unfavorable when comprehensively comparing the performance of MOFs in different projects. Third, due to the complicated structures and compositions of MOFs, the structure-activity relationship has not been clearly investigated and documented. Fourth, the exploration of more redox-active ligands is an urgent need for the development of novel electrocatalysis and electroensing methods. Lastly, the development of portable devices and simple operation is necessary for in situ and practical applications. Therefore, there are still many

undeveloped fields worthy of in-depth and systematic research, in view of the important value of MOFs for the development of electrochemical sensing platforms.

**Author Contributions:** Conceptualization, Y.C.; writing—original draft preparation, Y.C., J.L., L.Y. and M.L.; writing—review and editing, N.X.; project administration, L.L.; funding acquisition, L.L. All authors have read and agreed to the published version of the manuscript.

**Funding:** This research was funded by the Program for Innovative Research Team of Science and Technology in the University of Henan Province (21IRTSTHN005).

**Conflicts of Interest:** The authors declare no conflict of interest.

## References

1. Zhang, L.; Ying, Y.; Li, Y.; Fu, Y. Integration and synergy in protein-nanomaterial hybrids for biosensing: Strategies and in-field detection applications. *Biosens. Bioelectron.* **2020**, *154*, 112036–112045. [[CrossRef](#)] [[PubMed](#)]
2. Zhang, C.; Jiang, C.; Lan, L.; Ping, J.; Ye, Z.; Ying, Y. Nanomaterial-based biosensors for agro-product safety. *TrAC Trends Anal. Chem.* **2021**, *143*, 116369–116381. [[CrossRef](#)]
3. Kaur, H.; Shorie, M. Nanomaterial based aptasensors for clinical and environmental diagnostic applications. *Nanoscale Adv.* **2019**, *1*, 2123–2138. [[CrossRef](#)]
4. Zhao, Q.; Lu, D.; Zhang, G.; Zhang, D.; Shi, X. Recent improvements in enzyme-linked immunosorbent assays based on nanomaterials. *Talanta* **2021**, *223*, 121722–121737. [[CrossRef](#)]
5. Abolhasan, R.; Mehdizadeh, A.; Rashidi, M.R.; Aghebati-Maleki, L.; Yousefi, M. Application of hairpin DNA-based biosensors with various signal amplification strategies in clinical diagnosis. *Biosens. Bioelectron.* **2019**, *129*, 164–174. [[CrossRef](#)]
6. Chai, H.; Cheng, W.; Jin, D.; Miao, P. Recent progress in DNA hybridization chain reaction strategies for amplified biosensing. *ACS Appl. Mater. Interfaces* **2021**, *13*, 38931–38946. [[CrossRef](#)]
7. Ju, H. Functional nanomaterials and nanoprobe for amplified biosensing. *Appl. Mater. Today* **2018**, *10*, 51–71. [[CrossRef](#)]
8. Olorunyomi, J.F.; Geh, S.T.; Caruso, R.A.; Doherty, C.M. Metal-organic frameworks for chemical sensing devices. *Mater. Horiz.* **2021**, *8*, 2387–2419. [[CrossRef](#)]
9. Yuan, R.; Li, H.K.; He, H. Recent advances in metal/covalent organic framework-based electrochemical aptasensors for biosensing applications. *Dalton. Trans.* **2021**, *50*, 14091–14104. [[CrossRef](#)]
10. Yang, Z.; Zhang, W.; Yin, Y.; Fang, W.; Xue, H. Metal-organic framework-based sensors for the detection of toxins and foodborne pathogens. *Food Control* **2022**, *133*, 108684–108696. [[CrossRef](#)]
11. Cai, W.; Liu, X.; Wang, L.; Wang, B. Design and synthesis of noble metal-based electrocatalysts using metal-organic frameworks and derivatives. *Mater. Today Nano* **2022**, *17*, 100144–100164. [[CrossRef](#)]
12. Wu, H.B.; Lou, X.W. Metal-organic frameworks and their derived materials for electrochemical energy storage and conversion: Promises and challenges. *Sci. Adv.* **2017**, *3*, 9252–9268. [[CrossRef](#)] [[PubMed](#)]
13. Al Sharabati, M.; Sabouni, R.; Hussein, G.A. Biomedical applications of metal-organic frameworks for disease diagnosis and drug delivery: A review. *Nanomaterials* **2022**, *12*, 277. [[CrossRef](#)]
14. Yi, F.Y.; Chen, D.X.; Wu, M.K.; Han, L.; Jiang, H.L. Chemical sensors based on metal-organic frameworks. *ChemPlusChem* **2016**, *81*, 675–690. [[CrossRef](#)]
15. Pandey, M.D. Luminescent metal-organic frameworks as biosensors. *Mater. Lett.* **2022**, *308*, 131230. [[CrossRef](#)]
16. Marimuthu, M.; Arumugam, S.S.; Jiao, T.; Sabarinathan, D.; Li, H.; Chen, Q. Metal organic framework based sensors for the detection of food contaminants. *TrAC Trends Anal. Chem.* **2022**, *154*, 116642–116666. [[CrossRef](#)]
17. Kempahanumakkagari, S.; Vellingiri, K.; Deep, A.; Kwon, E.E.; Bolan, N.; Kim, K.H. Metal-organic framework composites as electrocatalysts for electrochemical sensing applications. *Coordin. Chem. Rev.* **2018**, *357*, 105–129. [[CrossRef](#)]
18. Carrasco, S. Metal-organic frameworks for the development of biosensors: A current overview. *Biosensors* **2018**, *8*, 92. [[CrossRef](#)]
19. Lv, M.; Zhou, W.; Tavakoli, H.; Bautista, C.; Xia, J.; Wang, Z.; Li, X. Aptamer-functionalized metal-organic frameworks (MOFs) for biosensing. *Biosens. Bioelectron.* **2021**, *176*, 112947–112963. [[CrossRef](#)]
20. Karimzadeh, Z.; Mahmoudpour, M.; Guardia, M.d.l.; Ezzati Nazhad Dolatabadi, J.; Jouyban, A. Aptamer-functionalized metal organic frameworks as an emerging nanoprobe in the food safety field: Promising development opportunities and translational challenges. *TrAC Trends Anal. Chem.* **2022**, *152*, 116622–116641. [[CrossRef](#)]
21. Zhang, X.L.; Li, G.L.; Wu, D.; Li, X.L.; Hu, N.; Chen, J.; Chen, G.; Wu, Y.N. Recent progress in the design fabrication of metal-organic frameworks-based nanozymes and their applications to sensing and cancer therapy. *Biosens. Bioelectron.* **2019**, *137*, 178–198. [[CrossRef](#)] [[PubMed](#)]
22. Wang, F.; Chen, L.; Liu, D.; Ma, W.; Dramou, P.; He, H. Nanozymes based on metal-organic frameworks: Construction and prospects. *TrAC Trends Anal. Chem.* **2020**, *133*, 116080–116096. [[CrossRef](#)]
23. Huang, X.; Zhang, S.; Tang, Y.; Zhang, X.; Bai, Y.; Pang, H. Advances in metal-organic framework-based nanozymes and their applications. *Coordin. Chem. Rev.* **2021**, *449*, 214216–214239. [[CrossRef](#)]

24. Mohan, B.; Kumar, S.; Xi, H.; Ma, S.; Tao, Z.; Xing, T.; You, H.; Zhang, Y.; Ren, P. Fabricated metal-organic frameworks (MOFs) as luminescent and electrochemical biosensors for cancer biomarkers detection. *Biosens. Bioelectron.* **2022**, *197*, 113738. [[CrossRef](#)] [[PubMed](#)]
25. Afreen, S.; He, Z.; Xiao, Y.; Zhu, J.J. Nanoscale metal-organic frameworks in detecting cancer biomarkers. *J. Mater. Chem. B* **2020**, *8*, 1338–1349. [[CrossRef](#)]
26. Anik, U.; Timur, S.; Dursun, Z. Metal organic frameworks in electrochemical and optical sensing platforms: A review. *Microchim. Acta* **2019**, *186*, 196–210. [[CrossRef](#)]
27. Sahoo, J.; Krishnaraj, C.; Sun, J.; Bihari Panda, B.; Subramanian, P.S.; Sekhar Jena, H. Lanthanide based inorganic phosphates and biological nucleotides sensor. *Coordin. Chem. Rev.* **2022**, *466*, 214583. [[CrossRef](#)]
28. Wang, Y.; Hu, Y.; He, Q.; Yan, J.; Xiong, H.; Wen, N.; Cai, S.; Peng, D.; Liu, Y.; Liu, Z. Metal-organic frameworks for virus detection. *Biosens. Bioelectron.* **2020**, *169*, 112604–112625. [[CrossRef](#)]
29. Gorle, D.B.; Ponnada, S.; Kiai, M.S.; Nair, K.K.; Nowduri, A.; Swart, H.C.; Ang, E.H.; Nanda, K.K. Review on recent progress in metal-organic framework-based materials for fabricating electrochemical glucose sensors. *J. Mater. Chem. B* **2021**, *9*, 7927–7954. [[CrossRef](#)]
30. Wang, X.; Wang, Y.; Ying, Y. Recent advances in sensing applications of metal nanoparticle/metal-organic framework composites. *TrAC Trends Anal. Chem.* **2021**, *143*, 116395–116415. [[CrossRef](#)]
31. Tajik, S.; Beitollahi, H.; Garkani Nejad, F.; Sheikhsheoie, I.; Nugraha, A.S.; Jang, H.W.; Yamauchi, Y.; Shokouhimehr, M. Performance of metal-organic frameworks in the electrochemical sensing of environmental pollutants. *J. Mater. Chem. A* **2021**, *9*, 8195–8220. [[CrossRef](#)]
32. Liu, S.; Lai, C.; Liu, X.; Li, B.; Zhang, C.; Qin, L.; Huang, D.; Yi, H.; Zhang, M.; Li, L.; et al. Metal-organic frameworks and their derivatives as signal amplification elements for electrochemical sensing. *Coordin. Chem. Rev.* **2020**, *424*, 213520–213537. [[CrossRef](#)]
33. Wang, Y.; Wu, Y.C.; Xie, J.; Hu, X.Y. Metal-organic framework modified carbon paste electrode for lead sensor. *Sens. Actuators B Chem.* **2013**, *177*, 1161–1166. [[CrossRef](#)]
34. Roushani, M.; Valipour, A.; Saedi, Z. Electroanalytical sensing of Cd<sup>2+</sup> based on metal-organic framework modified carbon paste electrode. *Sens. Actuators B Chem.* **2016**, *233*, 419–425. [[CrossRef](#)]
35. Jin, J.C.; Wu, J.; Yang, G.P.; Wu, Y.L.; Wang, Y.Y. A microporous anionic metal-organic framework for a highly selective and sensitive electrochemical sensor of Cu<sup>2+</sup> ions. *Chem. Commun.* **2016**, *52*, 8475–8478. [[CrossRef](#)]
36. Kajal, N.; Singh, V.; Gupta, R.; Gautam, S. Metal organic frameworks for electrochemical sensor applications: A review. *Environ. Res.* **2022**, *204*, 112320–112338. [[CrossRef](#)]
37. Li, Y.; Xie, M.; Zhang, X.; Liu, Q.; Lin, D.; Xu, C.; Xie, F.; Sun, X. Co-MOF nanosheet array: A high-performance electrochemical sensor for non-enzymatic glucose detection. *Sens. Actuators B Chem.* **2019**, *278*, 126–132. [[CrossRef](#)]
38. Zhao, F.; Sun, T.; Geng, F.; Chen, P.; Gao, Y. Metal-organic frameworks-based electrochemical sensors and biosensors. *Int. J. Electrochem. Sci.* **2019**, *14*, 5287–5304. [[CrossRef](#)]
39. Karimi-Harandi, M.-H.; Shabani-Nooshabadi, M.; Darabi, R. Cu-BTC metal-organic frameworks as catalytic modifier for ultrasensitive electrochemical determination of methocarbamol in the presence of methadone. *J. Electrochem. Soc.* **2021**, *168*, 097507–097516. [[CrossRef](#)]
40. Lopa, N.S.; Rahman, M.M.; Ahmed, F.; Sutradhar, S.C.; Ryu, T.; Kim, W. A base-stable metal-organic framework for sensitive and non-enzymatic electrochemical detection of hydrogen peroxide. *Electrochim. Acta* **2018**, *274*, 49–56. [[CrossRef](#)]
41. Zhang, D.; Zhang, X.; Bu, Y.; Zhang, J.; Zhang, R. Copper cobalt sulfide structures derived from MOF precursors with enhanced electrochemical glucose sensing properties. *Nanomaterials* **2022**, *12*, 1394. [[CrossRef](#)] [[PubMed](#)]
42. Gao, L.-L.; Gao, E.-Q. Metal-organic frameworks for electrochemical sensors of neurotransmitters. *Coordin. Chem. Rev.* **2021**, *434*, 213784–213795. [[CrossRef](#)]
43. Adeel, M.; Asif, K.; Rahman, M.M.; Daniele, S.; Canzonieri, V.; Rizzolio, F. Glucose detection devices and methods based on metal-organic frameworks and related materials. *Adv. Funct. Mater.* **2021**, *31*, 2106023–2106050. [[CrossRef](#)]
44. Daniel, M.; Mathew, G.; Anpo, M.; Neppolian, B. MOF based electrochemical sensors for the detection of physiologically relevant biomolecules: An overview. *Coordin. Chem. Rev.* **2022**, *468*, 214627–214661. [[CrossRef](#)]
45. Azizpour Moallem, Q.; Beitollahi, H. Electrochemical sensor for simultaneous detection of dopamine and uric acid based on a carbon paste electrode modified with nanostructured Cu-based metal-organic frameworks. *Microchem. J.* **2022**, *177*, 107261–107267. [[CrossRef](#)]
46. Li, Y.; Huangfu, C.; Du, H.; Liu, W.; Li, Y.; Ye, J. Electrochemical behavior of metal-organic framework MIL-101 modified carbon paste electrode: An excellent candidate for electroanalysis. *J. Electroanal. Chem.* **2013**, *709*, 65–69. [[CrossRef](#)]
47. Yang, L.; Xu, C.; Ye, W.; Liu, W. An electrochemical sensor for H<sub>2</sub>O<sub>2</sub> based on a new Co-metal-organic framework modified electrode. *Sens. Actuators B Chem.* **2015**, *215*, 489–496. [[CrossRef](#)]
48. Sohrabi, H.; Salahshour Sani, P.; Orooji, Y.; Majidi, M.R.; Yoon, Y.; Khataee, A. MOF-based sensor platforms for rapid detection of pesticides to maintain food quality and safety. *Food Chem. Toxicol.* **2022**, *165*, 113176–113192. [[CrossRef](#)]
49. Fang, X.; Zong, B.Y.; Mao, S. Metal-organic framework-based sensors for environmental contaminant sensing. *Nano-Micro Lett.* **2018**, *10*, 64–82. [[CrossRef](#)]
50. Manoj, D.; Rajendran, S.; Hoang, T.K.A.; Soto-Moscoso, M. The role of MOF based nanocomposites in the detection of phenolic compounds for environmental remediation- a review. *Chemosphere* **2022**, *300*, 134516–134529. [[CrossRef](#)]

51. Jiang, R.; Pang, Y.-H.; Yang, Q.-Y.; Wan, C.-Q.; Shen, X.-F. Copper porphyrin metal-organic framework modified carbon paper for electrochemical sensing of glyphosate. *Sens. Actuators B Chem.* **2022**, *358*, 131492–131500. [[CrossRef](#)]
52. Cao, Y.; Wang, L.; Shen, C.; Wang, C.; Hu, X.; Wang, G. An electrochemical sensor on the hierarchically porous Cu-BTC MOF platform for glyphosate determination. *Sens. Actuators B Chem.* **2019**, *283*, 487–494. [[CrossRef](#)]
53. Hu, Y.-w. Preparation of a Cu-MOF as an electrode modifier for the determination of carbendazim in water. *Int. J. Electrochem. Sci.* **2018**, *13*, 5031–5040. [[CrossRef](#)]
54. Dong, S.; Suo, G.; Li, N.; Chen, Z.; Peng, L.; Fu, Y.; Yang, Q.; Huang, T. A simple strategy to fabricate high sensitive 2,4-dichlorophenol electrochemical sensor based on metal organic framework Cu<sub>3</sub>(BTC)<sub>2</sub>. *Sens. Actuators B Chem.* **2016**, *222*, 972–979. [[CrossRef](#)]
55. Garg, N.; Deep, A.; Sharma, A.L. Recent trends and advances in porous metal-organic framework nanostructures for the electrochemical and optical sensing of heavy metals in water. *Crit. Rev. Anal. Chem.* **2022**, *52*, 1–25. [[CrossRef](#)]
56. Devaraj, M.; Sasikumar, Y.; Rajendran, S.; Ponce, L.C. Review—metal organic framework based nanomaterials for electrochemical sensing of toxic heavy metal ions: Progress and their prospects. *J. Electrochem. Soc.* **2021**, *168*, 037513–037522. [[CrossRef](#)]
57. Guo, H.X.; Zheng, Z.S.; Zhang, Y.H.; Lin, H.B.; Xu, Q.B. Highly selective detection of Pb<sup>2+</sup> by a nanoscale Ni-based metal-organic framework fabricated through one-pot hydrothermal reaction. *Sens. Actuators B Chem.* **2017**, *248*, 430–436. [[CrossRef](#)]
58. Niu, B.; Yao, B.; Zhu, M.; Guo, H.; Ying, S.; Chen, Z. Carbon paste electrode modified with fern leave-like MIL-47(as) for electrochemical simultaneous detection of Pb(II), Cu(II) and Hg(II). *J. Electroanal. Chem.* **2021**, *886*, 115121–115129. [[CrossRef](#)]
59. Zhou, Y.; Abazari, R.; Chen, J.; Tahir, M.; Kumar, A.; Ikreedeegh, R.R.; Rani, E.; Singh, H.; Kirillov, A.M. Bimetallic metal-organic frameworks and MOF-derived composites: Recent progress on electro- and photoelectrocatalytic applications. *Coord. Chem. Rev.* **2022**, *451*, 214264–214306. [[CrossRef](#)]
60. Rezki, M.; Septiani, N.L.W.; Iqbal, M.; Adhika, D.R.; Wenten, I.G.; Yulianto, B. Review—recent advance in multi-metallic metal organic frameworks (MM-MOFs) and their derivatives for electrochemical biosensor application. *J. Electrochem. Soc.* **2022**, *169*, 017504–017524. [[CrossRef](#)]
61. Du, Q.; Liao, Y.; Shi, N.; Sun, S.; Liao, X.; Yin, G.; Huang, Z.; Pu, X.; Wang, J. Facile synthesis of bimetallic metal-organic frameworks on nickel foam for a high performance non-enzymatic glucose sensor. *J. Electroanal. Chem.* **2022**, *904*, 115887–115894. [[CrossRef](#)]
62. Zou, H.; Tian, D.; Lv, C.; Wu, S.; Lu, G.; Guo, Y.; Liu, Y.; Yu, Y.; Ding, K. The synergistic effect of Co/Ni in ultrathin metal-organic framework nanosheets for the prominent optimization of non-enzymatic electrochemical glucose detection. *J. Mater. Chem. B* **2020**, *8*, 1008–1016. [[CrossRef](#)] [[PubMed](#)]
63. Tian, K.; Ma, Y.; Liu, Y.; Wang, M.; Guo, C.; He, L.; Song, Y.; Zhang, Z.; Du, M. Hierarchically structured hollow bimetallic ZnNi MOF microspheres as a sensing platform for adenosine detection. *Sens. Actuators B Chem.* **2020**, *303*, 127199–127207. [[CrossRef](#)]
64. Janjani, P.; Bhardwaj, U.; Gupta, R.; Singh Kushwaha, H. Bimetallic Mn/Fe MOF modified screen-printed electrodes for non-enzymatic electrochemical sensing of organophosphate. *Anal. Chim. Acta* **2022**, *1202*, 339676–339686. [[CrossRef](#)]
65. Huang, W.; Chen, Y.; Wu, L.; Long, M.; Lin, Z.; Su, Q.; Zheng, F.; Wu, S.; Li, H.; Yu, G. 3D Co-doped Ni-based conductive MOFs modified electrochemical sensor for highly sensitive detection of l-tryptophan. *Talanta* **2022**, *247*, 123596–123605. [[CrossRef](#)]
66. Li, Q.; Zheng, S.; Hu, X.; Shao, Z.; Zheng, M.; Pang, H. Ultrathin nanosheet Ni-metal organic framework assemblies for high-efficiency ascorbic acid electrocatalysis. *ChemElectroChem* **2018**, *5*, 3859–3865. [[CrossRef](#)]
67. Wang, Y.X.; Zhao, M.T.; Ping, J.F.; Chen, B.; Cao, X.H.; Huang, Y.; Tan, C.L.; Ma, Q.L.; Wu, S.X.; Yu, Y.F.; et al. Bioinspired design of ultrathin 2D bimetallic metal-organic-framework nanosheets used as biomimetic enzymes. *Adv. Mater.* **2016**, *28*, 4149–4155. [[CrossRef](#)]
68. Zeng, Z.R.; Fang, X.; Miao, W.; Liu, Y.; Maiyalagan, T.; Mao, S. Electrochemically sensing of trichloroacetic acid with iron(II) phthalocyanine and Zn-based metal organic framework nanocomposites. *ACS Sens.* **2019**, *4*, 1934–1941. [[CrossRef](#)]
69. Ko, M.; Mendecki, L.; Eagleton, A.M.; Durbin, C.G.; Stolz, R.M.; Meng, Z.; Mirica, K.A. Employing conductive metal-organic frameworks for voltammetric detection of neurochemicals. *J. Am. Chem. Soc.* **2020**, *142*, 11717–11733. [[CrossRef](#)]
70. Wei, C.; Zhou, H.; Liu, Q. PCN-222 MOF decorated conductive PEDOT films for sensitive electrochemical determination of chloramphenicol. *Mater. Chem. Phys.* **2021**, *270*, 124831–124839. [[CrossRef](#)]
71. Zhou, Z.; Mukherjee, S.; Hou, S.; Li, W.; Elsner, M.; Fischer, R.A. Porphyrinic MOF film for multifaceted electrochemical sensing. *Angew. Chem. Int. Ed.* **2021**, *60*, 20551–20557. [[CrossRef](#)] [[PubMed](#)]
72. Su, C.-H.; Kung, C.-W.; Chang, T.-H.; Lu, H.-C.; Ho, K.-C.; Liao, Y.-C. Inkjet-printed porphyrinic metal-organic framework thin films for electrocatalysis. *J. Mater. Chem. A* **2016**, *4*, 11094–11102. [[CrossRef](#)]
73. Liu, J.; Bo, X.; Li, M.; Yin, D.; Guo, L. Contrastive study on porphyrinic iron metal-organic framework supported on various carbon matrices as efficient electrocatalysts. *J. Colloid Interface Sci.* **2018**, *513*, 438–447. [[CrossRef](#)]
74. Xu, X.; Li, C.H.; Zhang, H.; Guo, X.M. Construction of electrochemical and photoelectrochemical sensing platform based on porphyrinic metal-organic frameworks for determination of ascorbic acid. *Nanomaterials* **2022**, *12*, 482. [[CrossRef](#)]
75. Xu, X.; Zhang, H.; Li, C.-H.; Guo, X.-M. Multimode determination of uric acid based on porphyrinic MOFs thin films by electrochemical and photoelectrochemical methods. *Microchem. J.* **2022**, *175*, 107198–107208. [[CrossRef](#)]
76. Kung, C.-W.; Chang, T.-H.; Chou, L.-Y.; Hupp, J.T.; Farha, O.K.; Ho, K.-C. Porphyrin-based metal-organic framework thin films for electrochemical nitrite detection. *Electrochem. Commun.* **2015**, *58*, 51–56. [[CrossRef](#)]

77. Meng, W.; Xu, S.; Dai, L.; Li, Y.H.; Zhu, J.; Wang, L. An enhanced sensitivity towards H<sub>2</sub>O<sub>2</sub> reduction based on a novel Cu metal-organic framework and acetylene black modified electrode. *Electrochim. Acta* **2017**, *230*, 324–332. [[CrossRef](#)]
78. Song, Y.H.; Xu, M.L.; Gong, C.C.; Shen, Y.; Wang, L.Y.; Xie, Y.; Wang, L. Ratiometric electrochemical glucose biosensor based on GOD/AuNPs/Cu-BTC MOFs/macroporous carbon integrated electrode. *Sens. Actuators B Chem.* **2018**, *257*, 792–799. [[CrossRef](#)]
79. Mokhtar, N.A.I.M.; Zawawi, R.M.; Khairul, W.M.; Yusof, N.A. Electrochemical and optical sensors made of composites of metal-organic frameworks and carbon-based materials. A review. *Environ. Chem. Lett.* **2022**. [[CrossRef](#)]
80. Wang, M.Q.; Zhang, Y.; Bao, S.J.; Yu, Y.N.; Ye, C. Ni(ii)-based metal-organic framework anchored on carbon nanotubes for highly sensitive non-enzymatic hydrogen peroxide sensing. *Electrochim. Acta* **2016**, *190*, 365–370. [[CrossRef](#)]
81. Chen, J.; Chen, Y.; Li, S.; Yang, J.; Dong, J. In-situ growth of cerium-based metal organic framework on multi-walled carbon nanotubes for electrochemical detection of gallic acid. *Colloid Surface. A* **2022**, *650*, 129318–129327. [[CrossRef](#)]
82. Mousaabadi, K.Z.; Ensafi, A.A.; Rezaei, B. Simultaneous determination of some opioid drugs using Cu-hemin MOF@MWCNTs as an electrochemical sensor. *Chemosphere* **2022**, *303*, 135149–135155. [[CrossRef](#)] [[PubMed](#)]
83. Weng, X.; Huang, J.; Ye, H.; Xu, H.; Cai, D.; Wang, D. A high-performance electrochemical sensor for sensitive detection of tetracycline based on a Zr-UiO-66/MWCNTs/AuNPs composite electrode. *Anal Methods* **2022**, *14*, 3000–3010. [[CrossRef](#)]
84. Du, Y.; Wang, B.; Kang, K.; Ji, X.; Wang, L.; Zhao, W.; Ren, J. Signal synergistic amplification strategy based on functionalized cemoFs for highly sensitive electrochemical detection of phenolic isomers. *Microchem. J.* **2022**, *177*, 107285–107294. [[CrossRef](#)]
85. Yan, Y.; Bo, X.; Guo, L. MOF-818 metal-organic framework-reduced graphene oxide/multiwalled carbon nanotubes composite for electrochemical sensitive detection of phenolic acids. *Talanta* **2020**, *218*, 121123–121130. [[CrossRef](#)] [[PubMed](#)]
86. Li, Y.; Shen, Y.; Zhang, Y.; Zeng, T.; Wan, Q.; Lai, G.; Yang, N. A UiO-66-NH<sub>2</sub>/carbon nanotube nanocomposite for simultaneous sensing of dopamine and acetaminophen. *Anal. Chim. Acta* **2021**, *1158*, 338419–338428. [[CrossRef](#)]
87. Wang, M.Q.; Ye, C.; Bao, S.J.; Zhang, Y.; Yu, Y.N.; Xu, M.W. Carbon nanotubes implanted manganese-based MOFs for simultaneous detection of biomolecules in body fluids. *Analyst.* **2016**, *141*, 1279–1285. [[CrossRef](#)]
88. Xu, C.; Liu, L.; Wu, C.; Wu, K. Unique 3D heterostructures assembled by quasi-2D Ni-MOF and CNTs for ultrasensitive electrochemical sensing of bisphenol A. *Sens. Actuators B Chem.* **2020**, *310*, 127885–127892. [[CrossRef](#)]
89. Rong, S.; Zou, L.; Meng, L.; Yang, X.; Dai, J.; Wu, M.; Qiu, R.; Tian, Y.; Feng, X.; Ren, X.; et al. Dual function metal-organic frameworks based ratiometric electrochemical sensor for detection of doxorubicin. *Anal. Chim. Acta* **2022**, *1196*, 339545–339552. [[CrossRef](#)]
90. Zhang, Y.Y.; Yan, P.; Wan, Q.J.; Yang, N.J. Integration of chromium terephthalate metal-organic frameworks with reduced graphene oxide for voltammetry of 4-nonylphenol. *Carbon* **2018**, *134*, 540–547. [[CrossRef](#)]
91. Wang, L.; Yang, H.; He, J.; Zhang, Y.Y.; Yu, J.; Song, Y.H. Cu-hemin metal-organic-frameworks/chitosan-reduced graphene oxide nanocomposites with peroxidase-like bioactivity for electrochemical sensing. *Electrochim. Acta* **2016**, *213*, 691–697. [[CrossRef](#)]
92. Wang, X.; Wang, Q.; Wang, Q.; Gao, F.; Gao, F.; Yang, Y.; Guo, H. Highly dispersible and stable copper terephthalate metal-organic framework-graphene oxide nanocomposite for an electrochemical sensing application. *ACS Appl. Mater. Interfaces* **2014**, *6*, 11573–11580. [[CrossRef](#)] [[PubMed](#)]
93. Mariyappan, V.; Chen, S.-M.; Jeyapragasam, T.; Devi, J.M. Designing and construction of a cobalt-metal-organic framework/heteroatoms co-doped reduced graphene oxide mesoporous nanocomposite based efficient electrocatalyst for chlorogenic acid detection. *J. Alloy. Compd.* **2022**, *898*, 163028–163039. [[CrossRef](#)]
94. Xie, Y.; Tu, X.L.; Ma, X.; Xiao, M.Q.; Liu, G.B.; Qu, F.L.; Dai, R.Y.; Lu, L.M.; Wang, W.M. In-situ synthesis of hierarchically porous polypyrrole@ZIF-8/graphene aerogels for enhanced electrochemical sensing of 2, 2-methylenebis (4-chlorophenol). *Electrochim. Acta* **2019**, *311*, 114–122. [[CrossRef](#)]
95. Lu, M.; Deng, Y.; Luo, Y.; Lv, J.; Li, T.; Xu, J.; Chen, S.W.; Wang, J. Graphene aerogel-metal-organic framework-based electrochemical method for simultaneous detection of multiple heavy-metal ions. *Anal. Chem.* **2019**, *91*, 888–895. [[CrossRef](#)] [[PubMed](#)]
96. Zhang, Y.; Bo, X.; Nsabimana, A.; Han, C.; Li, M.; Guo, L. Electrocatalytically active cobalt-based metal-organic framework with incorporated macroporous carbon composite for electrochemical applications. *J. Mater. Chem. A* **2015**, *3*, 732–738. [[CrossRef](#)]
97. Tang, J.; Liu, R.; Li, J.; Hui, Z.; Zheng, S.; Wu, J.; Guo, J.; Wang, X.; Wang, J. In situ growth of zeolitic imidazolate frameworks nanocrystals on ordered macroporous carbon for hydroquinone and catechol simultaneous determination. *J. Electrochem. Soc.* **2020**, *167*, 067504–067512. [[CrossRef](#)]
98. Wang, H.; Yuan, S.; Zhou, M.; Guo, L. A novel electrochemical sensor for detection of baicalein in human serum based on DUT-9/mesoporous carbon composite. *Electroanal.* **2019**, *32*, 648–655. [[CrossRef](#)]
99. Liu, J.; Bo, X.J.; Yang, J.; Yin, D.D.; Guo, L.P. One-step synthesis of porphyrinic iron-based metal-organic framework/ordered mesoporous carbon for electrochemical detection of hydrogen peroxide in living cells. *Sens. Actuators B Chem.* **2017**, *248*, 207–213. [[CrossRef](#)]
100. Wang, L.; Teng, Q.Q.; Sun, X.T.; Chen, Y.T.; Wang, Y.M.; Wang, H.; Zhang, Y.F. Facile synthesis of metal-organic frameworks/ordered mesoporous carbon composites with enhanced electrocatalytic ability for hydrazine. *J. Colloid Interface Sci.* **2018**, *512*, 127–133. [[CrossRef](#)]
101. Zhang, Y.; Jiang, J.; Zhang, Z.; Yu, H.; Rong, S.; Gao, H.; Pan, H.; Chang, D. Electrochemical strategy with zeolitic imidazolate framework-8 and ordered mesoporous carbon for detection of xanthine. *IET Nanobiotechnol.* **2020**, *14*, 120–125. [[CrossRef](#)] [[PubMed](#)]

102. Li, X.Y.; Li, C.L.; Wu, C.; Wu, K.B. Strategy for highly sensitive electrochemical sensing: In situ coupling of a metal-organic framework with ball-mill-exfoliated graphene. *Anal. Chem.* **2019**, *91*, 6043–6050. [[CrossRef](#)] [[PubMed](#)]
103. Zeng, Y.; Camarada, M.B.; Lu, X.; Tang, K.; Li, W.; Qiu, D.; Wen, Y.; Wu, G.; Luo, Q.; Bai, L. Detection and electrocatalytic mechanism of zearalenone using nanohybrid sensor based on copper-based metal-organic framework/magnetic Fe<sub>3</sub>O<sub>4</sub>-graphene oxide modified electrode. *Food Chem.* **2022**, *370*, 131024–131033. [[CrossRef](#)] [[PubMed](#)]
104. Xu, Y.; Yu, Y.; Xue, S.; Ma, X.; Tao, H. Innovative electrochemical sensor based on graphene oxide aerogel wrapped copper centered metal-organic framework to detect catechol. *J. Electroanal. Chem.* **2021**, *899*, 115686–115694. [[CrossRef](#)]
105. Li, C.; Wu, R.J.; Zou, J.C.; Zhang, T.T.; Zhang, S.F.; Zhang, Z.Q.; Hu, X.; Yan, Y.Q.; Ling, X.M. MNPs@anionic MOFs/ERGO with the size selectivity for the electrochemical determination of H<sub>2</sub>O<sub>2</sub> released from living cells. *Biosens. Bioelectron.* **2018**, *116*, 81–88. [[CrossRef](#)] [[PubMed](#)]
106. Chen, X.R.; Lau, D.; Cao, G.J.; Tang, Y.; Wu, C. In situ synthesis of a sandwich-like graphene@ZIF-67 heterostructure for highly sensitive nonenzymatic glucose sensing in human serums. *ACS Appl. Mater. Interfaces* **2019**, *11*, 9374–9384. [[CrossRef](#)]
107. Zhao, P.; Chen, S.; Zhou, J.; Zhang, S.; Huo, D.; Hou, C. A novel Fe-hemin-metal organic frameworks supported on chitosan-reduced graphene oxide for real-time monitoring of H<sub>2</sub>O<sub>2</sub> released from living cells. *Anal. Chim. Acta* **2020**, *1128*, 90–98. [[CrossRef](#)]
108. Wachholz Junior, D.; Deroco, P.B.; Kubota, L.T. A copper-based metal-organic framework/reduced graphene oxide-modified electrode for electrochemical detection of paraquat. *Microchim. Acta* **2022**, *189*, 278–289. [[CrossRef](#)]
109. Lin, J.; Hassan, M.; Bo, X.; Guo, L. Synthesis of iron-based metal-organic framework@large mesoporous carbon composites and their electrocatalytic properties. *J. Electroanal. Chem.* **2017**, *801*, 373–380. [[CrossRef](#)]
110. Yuan, S.; Bo, X.; Guo, L. In-situ growth of iron-based metal-organic framework crystal on ordered mesoporous carbon for efficient electrocatalysis of p-nitrotoluene and hydrazine. *Anal. Chim. Acta* **2018**, *1024*, 73–83. [[CrossRef](#)]
111. Rajpurohit, A.S.; Bora, D.K.; Srivastava, A.K. Simultaneous determination of amlodipine and losartan using an iron metal-organic framework/mesoporous carbon nanocomposite-modified glassy carbon electrode by differential pulse voltammetry. *Anal. Methods* **2018**, *10*, 5423–5438. [[CrossRef](#)]
112. Yan, Y.; Ma, J.; Bo, X.; Guo, L. Rod-like Co based metal-organic framework embedded into mesoporous carbon composite modified glassy carbon electrode for effective detection of pyrazinamide and isonicotinyl hydrazide in biological samples. *Talanta* **2019**, *205*, 120138–120147. [[CrossRef](#)] [[PubMed](#)]
113. Deng, M.; Lin, S.; Bo, X.; Guo, L. Simultaneous and sensitive electrochemical detection of dihydroxybenzene isomers with UiO-66 metal-organic framework/mesoporous carbon. *Talanta* **2017**, *174*, 527–538. [[CrossRef](#)] [[PubMed](#)]
114. Liu, C.; Bo, X.; Guo, L. A novel electrochemical sensing platform of JUC-62 metal-organic framework / platelet ordered mesoporous carbon for high selective detection of nitro-aromatic compounds. *Sens. Actuators B Chem.* **2019**, *297*, 126741–126752. [[CrossRef](#)]
115. Xu, Z.D.; Yang, L.Z.; Xu, C.L. Pt@UiO-66 heterostructures for highly selective detection of hydrogen peroxide with an extended linear range. *Anal. Chem.* **2015**, *87*, 3438–3444. [[CrossRef](#)]
116. Chen, H.Y.; Yang, T.; Liu, F.Q.; Li, W.H. Electrodeposition of gold nanoparticles on Cu-based metal-organic framework for the electrochemical detection of nitrite. *Sens. Actuators B Chem.* **2019**, *286*, 401–407. [[CrossRef](#)]
117. Liu, Y.; Weerasooriya, R.; Chen, X. The metal-organic framework supported gold nanoparticles as a highly sensitive platform for electrochemical detection of methyl mercury species in the aqueous environment. *J. Hazard. Mater.* **2022**, *431*, 128608–128617. [[CrossRef](#)]
118. Rani, R.; Deep, A.; Mizaikoff, B.; Singh, S. Zirconium metal organic framework based opto-electrochemical sensor for nitrofurazone detection. *J. Electroanal. Chem.* **2022**, *909*, 116124–116133. [[CrossRef](#)]
119. Chai, C.; Gao, J.; Zhao, G.; Li, L.; Tang, Y.; Wu, C.; Wan, C. In-situ synthesis of ultrasmall Au nanoparticles on bimetallic metal-organic framework with enhanced electrochemical activity for estrone sensing. *Anal. Chim. Acta* **2021**, *1152*, 338242–338248. [[CrossRef](#)]
120. Qiu, Z.; Yang, T.; Gao, R.; Jie, G.; Hou, W. An electrochemical ratiometric sensor based on 2D MOF nanosheet/Au/polyxanthurenic acid composite for detection of dopamine. *J. Electroanal. Chem.* **2019**, *835*, 123–129. [[CrossRef](#)]
121. da Silva, C.T.P.; Veregue, F.R.; Aguiar, L.W.; Meneguim, J.G.; Moisés, M.P.; Fávoro, S.L.; Radovanovic, E.; Giroto, E.M.; Rinaldi, A.W. Aunp@MOF composite as electrochemical material for determination of bisphenol A and its oxidation behavior study. *New J. Chem.* **2016**, *40*, 8872–8877. [[CrossRef](#)]
122. Mollarasouli, F.; Kurbanoglu, S.; Asadpour-Zeynali, K.; Ozkan, S.A. Preparation of porous Cu metal organic framework/ZnTe nanorods/Au nanoparticles hybrid platform for nonenzymatic determination of catechol. *J. Electroanal. Chem.* **2020**, *856*, 113672–113682. [[CrossRef](#)]
123. Wang, Y.; Wang, L.; Chen, H.H.; Hu, X.Y.; Ma, S.Q. Fabrication of highly sensitive and stable hydroxylamine electrochemical sensor based on gold nanoparticles and metal-metalloporphyrin framework modified electrode. *ACS Appl. Mater. Interfaces* **2016**, *8*, 18173–18181. [[CrossRef](#)] [[PubMed](#)]
124. Ling, P.; Cheng, S.; Chen, N.; Qian, C.; Gao, F. Nanozyme-modified metal-organic frameworks with multienzymes activity as biomimetic catalysts and electrocatalytic interfaces. *ACS Appl. Mater. Interfaces* **2020**, *12*, 17185–17192. [[CrossRef](#)]

125. Wang, Y.-C.; Chen, Y.-C.; Chuang, W.-S.; Li, J.-H.; Wang, Y.-S.; Chuang, C.-H.; Chen, C.-Y.; Kung, C.-W. Pore-confined silver nanoparticles in a porphyrinic metal–organic framework for electrochemical nitrite detection. *ACS Appl. Nano Mater.* **2020**, *3*, 9440–9448. [[CrossRef](#)]
126. Dong, Y.H.; Duan, C.Q.; Sheng, Q.L.; Zheng, J.B. Preparation of Ag@zeolitic imidazolate framework-67 at room temperature for electrochemical sensing of hydrogen peroxide. *Analyst* **2019**, *144*, 521–529. [[CrossRef](#)]
127. Zhang, W.; Jiang, T.; Sun, X.; Zhou, A.; Li, M. Determination of peracetic acid by an Ag nanoparticle decorated Cu-organic framework modified electrode. *Microchem. J.* **2021**, *171*, 106856–106863. [[CrossRef](#)]
128. Peng, X.; Wan, Y.; Wang, Y.; Liu, T.; Zou, P.; Wang, X.; Zhao, Q.; Ding, F.; Rao, H. Flower-like Ni(ii)-based metal-organic framework-decorated Ag nanoparticles: Fabrication, characterization and electrochemical detection of glucose. *Electroanalysis* **2019**, *31*, 2179–2186. [[CrossRef](#)]
129. Ma, J.; Bai, W.; Zheng, J. Non-enzymatic electrochemical hydrogen peroxide sensing using a nanocomposite prepared from silver nanoparticles and copper (ii)-porphyrin derived metal-organic framework nanosheets. *Microchim. Acta* **2019**, *186*, 482–489. [[CrossRef](#)]
130. Peng, Z.; Jiang, Z.; Huang, X.; Li, Y. A novel electrochemical sensor of tryptophan based on silver nanoparticles/metal–organic framework composite modified glassy carbon electrode. *RSC Adv.* **2016**, *6*, 13742–13748. [[CrossRef](#)]
131. Liu, T.; Zhou, M.; Pu, Y.; Liu, L.; Li, F.; Li, M.; Zhang, M. Silver nanoparticle-functionalized 3D flower-like copper (ii)-porphyrin framework nanocomposites as signal enhancers for fabricating a sensitive glutathione electrochemical sensor. *Sens. Actuators B Chem.* **2021**, *342*, 130047–130054. [[CrossRef](#)]
132. Fan, J.; Wang, H.; Zeng, X.; Su, L.; Zhang, X. An electrochemical sensor based on ZIF-67/Ag nanoparticles (NPs)/polydopamine (PDA) nanocomposites for detecting chloride ion with good reproducibility. *J. Electroanal. Chem.* **2022**, *914*, 116323–116329. [[CrossRef](#)]
133. Chen, Y.L.; Sun, X.; Biswas, S.; Xie, Y.; Wang, Y.; Hu, X.Y. Integrating polythiophene derivatives to PCN-222(Fe) for electrocatalytic sensing of L-dopa. *Biosens. Bioelectron.* **2019**, *141*, 111470–111477. [[CrossRef](#)]
134. Vinodh, R.; Babu, R.S.; Sambasivam, S.; Gopi, C.; Alzahmi, S.; Kim, H.J.; de Barros, A.L.F.; Obaidat, I.M. Recent advancements of polyaniline/metal organic framework (PANI/MOF) composite electrodes for supercapacitor applications: A critical review. *Nanomaterials* **2022**, *12*, 1511. [[CrossRef](#)] [[PubMed](#)]
135. Alsafrani, A.E.; Adeosun, W.A.; Marwani, H.M.; Khan, I.; Jawaid, M.; Asiri, A.M.; Khan, A. Efficient synthesis and characterization of polyaniline@aluminium-succinate metal-organic frameworks nanocomposite and its application for Zn(ii) ion sensing. *Polymers* **2021**, *13*, 3383. [[CrossRef](#)]
136. Zhou, K.; Shen, D.; Li, X.; Chen, Y.; Hou, L.; Zhang, Y.; Sha, J. Molybdenum oxide-based metal-organic framework/polypyrrole nanocomposites for enhancing electrochemical detection of dopamine. *Talanta* **2020**, *209*, 120507–120514. [[CrossRef](#)]
137. Liang, C.; Zhang, F.; Lin, H.; Jiang, C.; Guo, W.; Fan, S.; Qu, F. An innovative sensor for hydroxylamine determination: Using molybdenum hybrid zeolitic imidazolate framework–conducting polymer composite as electrocatalyst. *Electrochim. Acta* **2019**, *327*, 134945–134954. [[CrossRef](#)]
138. Chen, Y.L.; Huang, W.; Chen, K.J.; Zhang, T.; Wang, Y.; Wang, J.M. Facile fabrication of electrochemical sensor based on novel core-shell PPy@ZIF-8 structures: Enhanced charge collection for quercetin in human plasma samples. *Sens. Actuators B Chem.* **2019**, *290*, 434–442. [[CrossRef](#)]
139. Huang, T.Y.; Kung, C.W.; Liao, Y.T.; Kao, S.Y.; Cheng, M.; Chang, T.H.; Henzie, J.; Alamri, H.R.; Allothman, Z.A.; Yamauchi, Y.; et al. Enhanced charge collection in MOF-525-pedot nanotube composites enable highly sensitive biosensing. *Adv. Sci.* **2017**, *4*, 1700261–1700268. [[CrossRef](#)]
140. Wang, Y.; Wang, L.; Huang, W.; Zhang, T.; Hu, X.; Perman, J.A.; Ma, S. A metal–organic framework and conducting polymer based electrochemical sensor for high performance cadmium ion detection. *J. Mater. Chem. A* **2017**, *5*, 8385–8393. [[CrossRef](#)]
141. Xu, M.; Zhang, H.; Zheng, J. Polypyrrole microsphere modified porous UiO-66 for electrochemical nitrite sensing. *J. Electrochem. Soc.* **2022**, *169*, 047515–047520. [[CrossRef](#)]
142. Wang, N.; Zhao, W.; Shen, Z.; Sun, S.; Dai, H.; Ma, H.; Lin, M. Sensitive and selective detection of Pb (ii) and Cu (ii) using a metal-organic framework/polypyrrole nanocomposite functionalized electrode. *Sens. Actuators B Chem.* **2020**, *304*, 127286–127292. [[CrossRef](#)]
143. Wang, H.; Feng, X.; Bo, X.; Zhou, M.; Guo, L. Nickel-based metal-organic framework/crosslinked tubular poly(3,4-ethylenedioxythiophene) composite as an electrocatalyst for the detection of gallic acid and tinidazole. *ChemElectroChem* **2020**, *7*, 4031–4037. [[CrossRef](#)]
144. Liu, X.; Gao, X.; Yang, L.; Zhao, Y.; Li, F. Metal-organic framework-functionalized paper-based electrochemical biosensor for ultrasensitive exosome assay. *Anal. Chem.* **2021**, *93*, 11792–11799. [[CrossRef](#)] [[PubMed](#)]
145. Wang, Z.; Dong, P.; Sun, Z.X.; Sun, C.; Bu, H.Y.; Han, J.; Chen, S.P.; Xie, G. NH<sub>2</sub>-Ni-MOF electrocatalysts with tunable size/morphology for ultrasensitive C-reactive protein detection via an aptamer binding induced DNA walker-antibody sandwich assay. *J. Mater. Chem. B* **2018**, *6*, 2426–2431. [[CrossRef](#)]
146. Wang, F.; Gui, Y.; Liu, W.; Li, C.; Yang, Y. Precise molecular profiling of circulating exosomes using a metal-organic framework-based sensing interface and an enzyme-based electrochemical logic platform. *Anal. Chem.* **2022**, *94*, 875–883. [[CrossRef](#)]
147. Nemiwal, M.; Zhang, T.C.; Kumar, D. Enzyme immobilized nanomaterials as electrochemical biosensors for detection of biomolecules. *Enzyme Microb. Technol.* **2022**, *156*, 110006–110016. [[CrossRef](#)]

148. Dong, S.; Zhang, D.; Suo, G.; Wei, W.; Huang, T. Exploiting multi-function metal-organic framework nanocomposite Ag@Zn-TSA as highly efficient immobilization matrixes for sensitive electrochemical biosensing. *Anal. Chim. Acta* **2016**, *934*, 203–211. [[CrossRef](#)]
149. Kong, L.; Lv, S.; Qiao, Z.; Yan, Y.; Zhang, J.; Bi, S. Metal-organic framework nanoreactor-based electrochemical biosensor coupled with three-dimensional DNA walker for label-free detection of microRNA. *Biosens. Bioelectron.* **2022**, *207*, 114188–114195. [[CrossRef](#)]
150. Liang, W.; Wied, P.; Carraro, F.; Sumbly, C.J.; Nidetzky, B.; Tsung, C.K.; Falcaro, P.; Doonan, C.J. Metal-organic framework-based enzyme biocomposites. *Chem. Rev.* **2021**, *121*, 1077–1129. [[CrossRef](#)] [[PubMed](#)]
151. Lu, X.B.; Wang, X.; Wu, L.D.; Wu, L.X.; Dhanjai, Fu, L.; Gao, Y.; Chen, J.P. Response characteristics of bisphenols on a metal-organic framework-based tyrosinase nanosensor. *ACS Appl. Mater. Interfaces* **2016**, *8*, 16533–16539. [[CrossRef](#)]
152. Feng, Y.; Xu, Y.; Liu, S.; Wu, D.; Su, Z.; Chen, G.; Liu, J.; Li, G. Recent advances in enzyme immobilization based on novel porous framework materials and its applications in biosensing. *Coordin. Chem. Rev.* **2022**, *459*, 214414–214440. [[CrossRef](#)]
153. Wang, Q.; Lian, X.Z.; Fang, Y.; Zhou, H.C. Applications of immobilized bio-catalyst in metal-organic frameworks. *Catalysts* **2018**, *8*, 166. [[CrossRef](#)]
154. Mehta, J.; Bhardwaj, N.; Bhardwaj, S.K.; Kim, K.-H.; Deep, A. Recent advances in enzyme immobilization techniques: Metal-organic framework materials as novel substrates. *Coordin. Chem. Rev.* **2016**, *322*, 30–40. [[CrossRef](#)]
155. Huang, W.; Huang, S.; Chen, G.; Ouyang, G. Biocatalytic metal-organic frameworks: Promising materials for biosensing. *ChemBioChem* **2022**, *23*, e202100567. [[CrossRef](#)] [[PubMed](#)]
156. Cheng, X.; Zhou, J.; Chen, J.; Xie, Z.; Kuang, Q.; Zheng, L. One-step synthesis of thermally stable artificial multienzyme cascade system for efficient enzymatic electrochemical detection. *Nano Res.* **2019**, *12*, 3031–3036. [[CrossRef](#)]
157. Singh, R.; Musameh, M.; Gao, Y.; Ozcelik, B.; Mulet, X.; Doherty, C.M. Stable MOF@enzyme composites for electrochemical biosensing devices. *J. Mater. Chem. C* **2021**, *9*, 7677–7688. [[CrossRef](#)]
158. Zhang, Q.; Zhang, L.; Dai, H.; Li, Z.; Fu, Y.; Li, Y. Biomineralization-mimetic preparation of robust metal-organic frameworks biocomposites film with high enzyme load for electrochemical biosensing. *J. Electroanal. Chem.* **2018**, *823*, 40–46. [[CrossRef](#)]
159. Wang, Y.; Hou, C.; Zhang, Y.; He, F.; Liu, M.Z.; Li, X.L. Preparation of graphene nano-sheet bonded PDA/MOF microcapsules with immobilized glucose oxidase as a mimetic multi-enzyme system for electrochemical sensing of glucose. *J. Mater. Chem. B* **2016**, *4*, 3695–3702. [[CrossRef](#)]
160. Paul, A.; Vyas, G.; Paul, P.; Srivastava, D.N. Gold-nanoparticle-encapsulated ZIF-8 for a mediator-free enzymatic glucose sensor by amperometry. *ACS Appl. Nano Mater.* **2018**, *1*, 3600–3607. [[CrossRef](#)]
161. Song, Y.; Shen, Y.; Gong, C.; Chen, J.; Xu, M.; Wang, L.; Wang, L. A novel glucose biosensor based on Tb@mesoporous metal-organic frameworks/carbon nanotube nanocomposites. *ChemElectroChem* **2017**, *4*, 1457–1462. [[CrossRef](#)]
162. Ma, W.; Jiang, Q.; Yu, P.; Yang, L.; Mao, L. Zeolitic imidazolate framework-based electrochemical biosensor for in vivo electrochemical measurements. *Anal. Chem.* **2013**, *85*, 7550–7557. [[CrossRef](#)] [[PubMed](#)]
163. Lyu, F.; Zhang, Y.; Zare, R.N.; Ge, J.; Liu, Z. One-pot synthesis of protein-embedded metal-organic frameworks with enhanced biological activities. *Nano Lett.* **2014**, *14*, 5761–5765. [[CrossRef](#)]
164. Wang, Q.; Chen, M.; Xiong, C.; Zhu, X.; Chen, C.; Zhou, F.; Dong, Y.; Wang, Y.; Xu, J.; Li, Y.; et al. Dual confinement of high-loading enzymes within metal-organic frameworks for glucose sensor with enhanced cascade biocatalysis. *Biosens. Bioelectron.* **2022**, *196*, 113695–113701. [[CrossRef](#)] [[PubMed](#)]
165. Liu, X.; Chen, W.; Lian, M.; Chen, X.; Lu, Y.; Yang, W. Enzyme immobilization on ZIF-67/MWCNT composite engenders high sensitivity electrochemical sensing. *J. Electroanal. Chem.* **2019**, *833*, 505–511. [[CrossRef](#)]
166. Chen, W.; Yang, W.; Lu, Y.; Zhu, W.; Chen, X. Encapsulation of enzyme into mesoporous cages of metal-organic frameworks for the development of highly stable electrochemical biosensors. *Anal. Methods* **2017**, *9*, 3213–3220. [[CrossRef](#)]
167. Fan, Z.; Wang, J.; Nie, Y.; Ren, L.; Liu, B.; Liu, G. Metal-organic frameworks/graphene oxide composite: A new enzymatic immobilization carrier for hydrogen peroxide biosensors. *J. Electrochem. Soc.* **2015**, *163*, B32–B37. [[CrossRef](#)]
168. Xu, M. A novel H<sub>2</sub>O<sub>2</sub> biosensor based on the composite of MP-11 encapsulated in PCN-333(Al)-graphene oxide. *Int. J. Electrochem. Sci.* **2017**, *12*, 10390–10401. [[CrossRef](#)]
169. Gong, C.; Shen, Y.; Chen, J.; Song, Y.; Chen, S.; Song, Y.; Wang, L. Microperoxidase-11@PCN-333 (Al)/three-dimensional macroporous carbon electrode for sensing hydrogen peroxide. *Sens. Actuators B Chem.* **2017**, *239*, 890–897. [[CrossRef](#)]
170. Zhang, C.; Wang, X.R.; Hou, M.; Li, X.Y.; Wu, X.L.; Ge, J. Immobilization on metal-organic framework engenders high sensitivity for enzymatic electrochemical detection. *ACS Appl. Mater. Interfaces* **2017**, *9*, 13831–13836. [[CrossRef](#)]
171. Wen, Y.; Li, R.; Liu, J.; Zhang, X.; Wang, P.; Zhang, X.; Zhou, B.; Li, H.; Wang, J.; Li, Z.; et al. Promotion effect of Zn on 2D bimetallic NiZn metal organic framework nanosheets for tyrosinase immobilization and ultrasensitive detection of phenol. *Anal. Chim. Acta* **2020**, *1127*, 131–139. [[CrossRef](#)] [[PubMed](#)]
172. Wang, X.; Lu, X.; Wu, L.; Chen, J. 3D metal-organic framework as highly efficient biosensing platform for ultrasensitive and rapid detection of bisphenol A. *Biosens. Bioelectron.* **2015**, *65*, 295–301. [[CrossRef](#)] [[PubMed](#)]
173. Ponnada, S.; Gorle, D.B.; Kiai, M.S.; Raju, C.V.; Faraji, M.; Sharma, R.K.; Nowduri, A. Understanding the endocrine disruptor and determination of bisphenol A by functional Cu-BTABB-MOF/rGO composite as facile rapid electrochemical sensor: An experimental and DFT investigation. *Anal Methods* **2022**, *14*, 560–573. [[CrossRef](#)] [[PubMed](#)]

174. Ma, J.; Yuan, J.; Xu, Y.; Jiang, Y.; Bai, W.; Zheng, J. Ultrasensitive electrochemical determination of bisphenol A in food samples based on a strategy for activity enhancement of enzyme: Layer-by-layer self-assembly of tyrosinase between two-dimensional porphyrin metal-organic framework nanofilms. *Chem. Eng. J.* **2022**, *446*, 137001–137012. [[CrossRef](#)]
175. Li, S.; He, B.; Liang, Y.; Wang, J.; Jiao, Q.; Liu, Y.; Guo, R.; Wei, M.; Jin, H. Sensitive electrochemical aptasensor for determination of sulfaquinolone based on AuPd NPs@UiO-66-NH<sub>2</sub>/CoSe<sub>2</sub> and RecJf exonuclease-assisted signal amplification. *Anal. Chim. Acta* **2021**, *1182*, 338948–338957. [[CrossRef](#)]
176. Qin, X.; Wang, B.; Li, X.; Ding, Y.; Yang, X.; Zhou, Y.; Xu, W.; Xu, M.; Gu, C. Toluidine blue-assisted synthesis of functionalized M (M = Cu, Co, Zn)-metal-organic frameworks for electrochemical immunoassay of proteins. *J. Electroanal. Chem.* **2022**, *911*, 116186–116193. [[CrossRef](#)]
177. Zhou, N.; Su, F.F.; Guo, C.P.; He, L.H.; Jia, Z.K.; Wang, M.H.; Jia, Q.J.; Zhang, Z.H.; Lu, S.Y. Two-dimensional oriented growth of Zn-MOF-on-Zr-MOF architecture: A highly sensitive and selective platform for detecting cancer markers. *Biosens. Bioelectron.* **2019**, *123*, 51–58. [[CrossRef](#)]
178. Ehzari, H.; Samimi, M.; Safari, M.; Gholivand, M.B. Label-free electrochemical immunosensor for sensitive HER2 biomarker detection using the core-shell magnetic metal-organic frameworks. *J. Electroanal. Chem.* **2020**, *877*, 114722–114731. [[CrossRef](#)]
179. Hu, M.; Hu, X.F.; Zhang, Y.P.; Teng, M.; Deng, R.G.; Xing, G.X.; Tao, J.Z.; Xu, G.R.; Chen, J.; Zhang, Y.J.; et al. Label-free electrochemical immunosensor based on AuNPs/Zn/Ni-ZIF-8-800@graphene composites for sensitive detection of monensin in milk. *Sens. Actuators B Chem.* **2019**, *288*, 571–578. [[CrossRef](#)]
180. Liu, C.S.; Sun, C.X.; Tian, J.Y.; Wang, Z.W.; Ji, H.F.; Song, Y.P.; Zhang, S.; Zhang, Z.H.; He, L.H.; Du, M. Highly stable aluminum-based metal-organic frameworks as biosensing platforms for assessment of food safety. *Biosens. Bioelectron.* **2017**, *91*, 804–810. [[CrossRef](#)]
181. Biswas, S.; Lan, Q.; Xie, Y.; Sun, X.; Wang, Y. Label-free electrochemical immunosensor for ultrasensitive detection of carbohydrate antigen 125 based on antibody-immobilized biocompatible MOF-808/CNT. *ACS Appl. Mater. Interfaces* **2021**, *13*, 3295–3302. [[CrossRef](#)] [[PubMed](#)]
182. Li, L.; Liu, X.; Su, B.; Zhang, H.; Li, R.; Liu, Z.; Chen, Q.; Huang, T.; Cao, H. An innovative electrochemical immunosensor based on nanobody heptamer and AuNPs@ZIF-8 nanocomposites as support for the detection of alpha fetoprotein in serum. *Microchem. J.* **2022**, *179*, 107463–107471. [[CrossRef](#)]
183. Duan, F.; Rong, F.; Guo, C.; Chen, K.; Wang, M.; Zhang, Z.; Pettinari, R.; Zhou, L.; Du, M. Electrochemical aptasensing strategy based on a multivariate polymertitanium-metal-organic framework for zearalenone analysis. *Food Chem.* **2022**, *385*, 132654–132663. [[CrossRef](#)] [[PubMed](#)]
184. Liu, C.S.; Zhang, Z.H.; Chen, M.; Zhao, H.; Duan, F.H.; Chen, D.M.; Wang, M.H.; Zhang, S.; Du, M. Pore modulation of zirconium-organic frameworks for high-efficiency detection of trace proteins. *Chem. Commun.* **2017**, *53*, 3941–3944. [[CrossRef](#)]
185. Su, F.F.; Zhang, S.; Ji, H.F.; Zhao, H.; Tian, J.Y.; Liu, C.S.; Zhang, Z.H.; Fang, S.M.; Zhu, X.L.; Du, M. Two-dimensional zirconium-based metal organic framework nanosheet composites embedded with Au nanoclusters: A highly sensitive electrochemical aptasensor toward detecting cocaine. *ACS Sens.* **2017**, *2*, 998–1005. [[CrossRef](#)] [[PubMed](#)]
186. Zhang, Z.H.; Duan, F.H.; Tian, J.Y.; He, J.Y.; Yang, L.Y.; Zhao, H.; Zhang, S.; Liu, C.S.; He, L.H.; Chen, M.; et al. Aptamer-embedded zirconium-based metal-organic framework composites prepared by de novo bio-inspired approach with enhanced biosensing for detecting trace analytes. *ACS Sens.* **2017**, *2*, 982–989. [[CrossRef](#)]
187. Sun, Z.; Peng, Y.; Wang, M.; Lin, Y.; Jalalah, M.; Alsareii, S.A.; Harraz, F.A.; Yang, J.; Li, G. Electrochemical deposition of Cu metal-organic framework films for the dual analysis of pathogens. *Anal. Chem.* **2021**, *93*, 8994–9001. [[CrossRef](#)]
188. Rezki, M.; Septiani, N.L.W.; Iqbal, M.; Harimurti, S.; Sambegoro, P.; Adhika, D.R.; Yulianto, B. Amine-functionalized Cu-MOF nanospheres towards label-free hepatitis B surface antigen electrochemical immunosensors. *J. Mater. Chem. B* **2021**, *9*, 5711–5721. [[CrossRef](#)]
189. Xing, G.; Wang, C.; Liu, K.; Luo, B.; Hou, P.; Wang, X.; Dong, H.; Wang, J.; Li, A. A probe-free electrochemical immunosensor for methyl jasmonate based on a Cu-MOF-carboxylated graphene oxide platform. *RSC Adv.* **2022**, *12*, 16688–16695. [[CrossRef](#)]
190. Li, H.; Qi, H.; Chang, J.; Gai, P.; Li, F. Recent progress in homogeneous electrochemical sensors and their designs and applications. *TrAC Trends Anal. Chem.* **2022**, *156*, 116622–116636. [[CrossRef](#)]
191. Wang, Z.; Zhang, Y.; Wang, X.; Han, L. Flow-homogeneous electrochemical sensing system based on 2D metal-organic framework nanozyme for successive microRNA assay. *Biosens. Bioelectron.* **2022**, *206*, 114120–114128. [[CrossRef](#)] [[PubMed](#)]
192. Ahmadi, A.; Khoshfetrat, S.M.; Mirzaeizadeh, Z.; Kabiri, S.; Rezaie, J.; Omidfar, K. Electrochemical immunosensor for determination of cardiac troponin I using two-dimensional metal-organic framework/Fe<sub>3</sub>O<sub>4</sub>-COOH nanosheet composites loaded with thionine and pCTAB/DES modified electrode. *Talanta* **2022**, *237*, 122911–122918. [[CrossRef](#)]
193. He, B.S.; Dong, X.Z. Hierarchically porous Zr-MOFs labelled methylene blue as signal tags for electrochemical patulin aptasensor based on ZnO nano flower. *Sens. Actuators B Chem.* **2019**, *294*, 192–198. [[CrossRef](#)]
194. Lv, M.; Cao, X.; Tian, M.; Jiang, R.; Gao, C.; Xia, J.; Wang, Z. A novel electrochemical biosensor based on MIL-101-NH<sub>2</sub> (Cr) combining target-responsive releasing and self-catalysis strategy for p53 detection. *Biosens. Bioelectron.* **2022**, *214*, 114518–114524. [[CrossRef](#)]
195. Zheng, Q.; Wang, T.; Li, X.; Qian, H.; Bian, X.; Li, X.; Bai, H.; Ding, S.; Yan, Y. Femtomolar and locus-specific detection of N(6)-methyladenine in DNA by integrating double-hindered replication and nucleic acid-functionalized MB@Zr-MOF. *J. Nanobiotechnol.* **2021**, *19*, 408–418. [[CrossRef](#)] [[PubMed](#)]

196. Miao, J.; Du, K.; Li, X.; Xu, X.; Dong, X.; Fang, J.; Cao, W.; Wei, Q. Ratiometric electrochemical immunosensor for the detection of procalcitonin based on the ratios of SiO<sub>2</sub>-Fc-COOH-Au and UiO-66-TB complexes. *Biosens. Bioelectron.* **2021**, *171*, 112713–112719. [[CrossRef](#)]
197. Gu, C.; Bai, L.; Pu, L.; Gai, P.; Li, F. Highly sensitive and stable self-powered biosensing for exosomes based on dual metal-organic frameworks nanocarriers. *Biosens. Bioelectron.* **2021**, *176*, 112907–112912. [[CrossRef](#)] [[PubMed](#)]
198. Han, J.; Zhang, M.F.; Chen, G.J.; Zhang, Y.Q.; Wei, Q.; Zhuo, Y.; Xie, G.; Yuan, R.; Chen, S.P. Ferrocene covalently confined in porous MOF as signal tag for highly sensitive electrochemical immunoassay of amyloid-beta. *J. Mater. Chem. B* **2017**, *5*, 8330–8336. [[CrossRef](#)] [[PubMed](#)]
199. Li, M.; Xia, X.; Meng, S.; Ma, Y.; Yang, T.; Yang, Y.; Hu, R. An electrochemical immunosensor coupling a bamboo-like carbon nanostructure substrate with toluidine blue-functionalized Cu(II)-MOFs as signal probes for a C-reactive protein assay. *RSC Adv.* **2021**, *11*, 6699–6708. [[CrossRef](#)]
200. Sun, Z.; Wang, L.; Wu, S.; Pan, Y.; Dong, Y.; Zhu, S.; Yang, J.; Yin, Y.; Li, G. An electrochemical biosensor designed by using Zr-based metal-organic frameworks for the detection of glioblastoma-derived exosomes with practical application. *Anal. Chem.* **2020**, *92*, 3819–3826. [[CrossRef](#)]
201. Zhang, B.; Lv, L.; Ma, X.; Xie, L.; Lin, M.; Chen, H.; He, B. Au@ZnNi-MOF labeled electrochemical aptasensor for detection of enrofloxacin based on AuPt@h-CeO<sub>2</sub>/MoS<sub>2</sub> and DNAzyme-driven DNA walker triple amplification signal strategy. *Biosens. Bioelectron.* **2022**, *210*, 114296–114303. [[CrossRef](#)] [[PubMed](#)]
202. Liu, J.; Liu, J.; Shang, Y.; Xu, J.; Wang, X.; Zheng, J. An electrochemical immunosensor for simultaneous detection of two lung cancer markers based on electroactive probes. *J. Electroanal. Chem.* **2022**, *919*, 116559–116565. [[CrossRef](#)]
203. Huang, S.; Gan, N.; Li, T.; Zhou, Y.; Cao, Y.; Dong, Y. Electrochemical aptasensor for multi-antibiotics detection based on endonuclease and exonuclease assisted dual recycling amplification strategy. *Talanta* **2018**, *179*, 28–36. [[CrossRef](#)] [[PubMed](#)]
204. Chang, J.; Wang, X.; Wang, J.; Li, H.; Li, F. Nucleic acid-functionalized metal-organic framework-based homogeneous electrochemical biosensor for simultaneous detection of multiple tumor biomarkers. *Anal. Chem.* **2019**, *91*, 3604–3610. [[CrossRef](#)] [[PubMed](#)]
205. Yang, Y.; Cheng, J.; Wang, B.; Guo, Y.; Dong, X.; Zhao, J. An amino-modified metal-organic framework (type UiO-66-NH<sub>2</sub>) loaded with cadmium(II) and lead(II) ions for simultaneous electrochemical immunosensing of triazophos and thiacloprid. *Microchim. Acta* **2019**, *186*, 101–110. [[CrossRef](#)]
206. Chen, M.; Gan, N.; Zhou, Y.; Li, T.; Xu, Q.; Cao, Y.; Chen, Y. An electrochemical aptasensor for multiplex antibiotics detection based on metal ions doped nanoscale MOFs as signal tracers and RecJf exonuclease-assisted targets recycling amplification. *Talanta* **2016**, *161*, 867–874. [[CrossRef](#)]
207. Chen, M.; Gan, N.; Zhou, Y.; Li, T.; Xu, Q.; Cao, Y.; Chen, Y. A novel aptamer-metal ions-nanoscale MOF based electrochemical biocodes for multiple antibiotics detection and signal amplification. *Sens. Actuators B Chem.* **2017**, *242*, 1201–1209. [[CrossRef](#)]
208. Zhou, Y.; Wei, L.; Chen, L. Application of metal-organic framework (MOF)-based enzymatic amplification strategy for the sensitive electrochemical detection of tuberculosis. *Sens. Actuators B Chem.* **2020**, *324*, 128724–128732. [[CrossRef](#)]
209. Chen, J.; Yu, C.; Zhao, Y.L.; Niu, Y.Z.; Zhang, L.; Yu, Y.J.; Wu, J.; He, J.L. A novel non-invasive detection method for the FGFR3 gene mutation in maternal plasma for a fetal achondroplasia diagnosis based on signal amplification by hemin-MOFs/PtNPs. *Biosens. Bioelectron.* **2017**, *91*, 892–899. [[CrossRef](#)]
210. Ling, P.; Lei, J.; Zhang, L.; Ju, H. Porphyrin-encapsulated metal-organic frameworks as mimetic catalysts for electrochemical DNA sensing via allosteric switch of hairpin DNA. *Anal. Chem.* **2015**, *87*, 3957–3963. [[CrossRef](#)]
211. Xie, S.; Ye, J.; Yuan, Y.; Chai, Y.; Yuan, R. A multifunctional hemin@metal-organic framework and its application to construct an electrochemical aptasensor for thrombin detection. *Nanoscale* **2015**, *7*, 18232–18238. [[CrossRef](#)] [[PubMed](#)]
212. Zheng, Y.; Ma, Z. Multifunctionalized zifs nanoprobe-initiated tandem reaction for signal amplified electrochemical immunoassay of carbohydrate antigen 24-2. *Biosens. Bioelectron.* **2019**, *129*, 42–49. [[CrossRef](#)] [[PubMed](#)]
213. Tian, J.; Liang, Z.; Hu, O.; He, Q.; Sun, D.; Chen, Z. An electrochemical dual-aptamer biosensor based on metal-organic frameworks MIL-53 decorated with Au@Pt nanoparticles and enzymes for detection of COVID-19 nucleocapsid protein. *Electrochim. Acta* **2021**, *387*, 138553–138560. [[CrossRef](#)]
214. Ou, D.; Sun, D.; Liang, Z.; Chen, B.; Lin, X.; Chen, Z. A novel cytosensor for capture, detection and release of breast cancer cells based on metal organic framework PCN-224 and DNA tetrahedron linked dual-aptamer. *Sens. Actuators B Chem.* **2019**, *285*, 398–404. [[CrossRef](#)]
215. Liu, Z.; Wang, X.; Dong, F.; Li, Y.; Guo, Y.; Liu, X.; Xu, J.; Wu, X.; Zheng, Y. Ultrasensitive immunoassay for detection of zearalenone in agro-products using enzyme and antibody co-embedded zeolitic imidazolate framework as labels. *J. Hazard. Mater.* **2021**, *412*, 125276–125284. [[CrossRef](#)]
216. Li, W.; Chen, S.; Yang, Y.; Song, Y.; Ma, C.; Qiao, X.; Hong, C. Ultrasensitive electrochemical immunosensor based on the signal amplification strategy of the competitive reaction of Zn<sup>2+</sup> and ATP ions to construct a “signal on” mode GOx-HRP enzyme cascade reaction. *Microchim. Acta* **2021**, *188*, 61–69. [[CrossRef](#)]
217. Feng, J.; Liang, X.; Ma, Z. New immunoprobe: Dual-labeling ZIF-8 embellished with multifunctional bovine serum albumin lamella for electrochemical immunoassay of tumor marker. *Biosens. Bioelectron.* **2021**, *175*, 112853–112858. [[CrossRef](#)]

218. Zhang, C.L.; He, J.L.; Zhang, Y.C.; Chen, J.; Zhao, Y.L.; Niu, Y.Z.; Yu, C. Cerium dioxide-doped carboxyl fullerene as novel nanoprobe and catalyst in electrochemical biosensor for amperometric detection of the CYP2C19\*2 allele in human serum. *Biosens. Bioelectron.* **2018**, *102*, 94–100. [[CrossRef](#)]
219. Zhao, H.; Du, X.; Dong, H.; Jin, D.; Tang, F.; Liu, Q.; Wang, P.; Chen, L.; Zhao, P.; Li, Y. Electrochemical immunosensor based on Au/Co-BDC/MoS<sub>2</sub> and DPCN/MoS<sub>2</sub> for the detection of cardiac troponin I. *Biosens. Bioelectron.* **2021**, *175*, 112883–112890. [[CrossRef](#)]
220. Wang, Z.; Yu, H.; Han, J.; Xie, G.; Chen, S.P. Rare Co/Fe-MOFs exhibiting high catalytic activity in electrochemical aptasensors for ultrasensitive detection of ochratoxin A. *Chem. Commun.* **2017**, *53*, 9926–9929. [[CrossRef](#)]
221. Chen, Y.H.; Liu, X.Z.; Guo, S.L.; Cao, J.; Zhou, J.; Zuo, J.L.; Bai, L.J. A sandwich-type electrochemical aptasensor for mycobacterium tuberculosis MPT64 antigen detection using C(60)NPs decorated N-CNTs/GO nanocomposite coupled with conductive pei-functionalized metal-organic framework. *Biomaterials.* **2019**, *216*, 119253–119262. [[CrossRef](#)]
222. Zhong, M.; Yang, L.; Yang, H.; Cheng, C.; Deng, W.; Tan, Y.; Xie, Q.; Yao, S. An electrochemical immunobiosensor for ultrasensitive detection of Escherichia coli o157:H7 using CdS quantum dots-encapsulated metal-organic frameworks as signal-amplifying tags. *Biosens. Bioelectron.* **2019**, *126*, 493–500. [[CrossRef](#)] [[PubMed](#)]
223. Wang, Y.; Dong, P.; Huang, J.; Xu, H.; Lei, J.; Zhang, L. Direct electrochemistry of silver nanoparticles-decorated metal-organic frameworks for telomerase activity sensing via allosteric activation of an aptamer hairpin. *Anal. Chim. Acta* **2021**, *1184*, 339036–339045. [[CrossRef](#)] [[PubMed](#)]
224. Li, W.; Yang, Y.; Ma, C.; Song, Y.; Hong, C.; Qiao, X. A sandwich-type electrochemical immunosensor for ultrasensitive detection of CEA based on core-shell Cu<sub>2</sub>O@Cu-MOF@Au NPs nanostructure attached with HRP for triple signal amplification. *J. Mater. Sci.* **2020**, *55*, 13980–13994. [[CrossRef](#)]
225. Zhang, J.; Xu, X.; Qiang, Y. Ultrasensitive electrochemical aptasensor for ochratoxin A detection using AgPt bimetallic nanoparticles decorated iron-porphyrinic metal-organic framework for signal amplification. *Sens. Actuators B Chem.* **2020**, *312*, 127964–127971. [[CrossRef](#)]
226. Wang, L.; Meng, T.; Liang, L.; Sun, J.; Wu, S.; Wang, H.; Yang, X.; Zhang, Y. Fabrication of amine-functionalized metal-organic frameworks with embedded palladium nanoparticles for highly sensitive electrochemical detection of telomerase activity. *Sens. Actuators B Chem.* **2019**, *278*, 133–139. [[CrossRef](#)]
227. Meng, T.; Shang, N.; Nsabimana, A.; Ye, H.; Wang, H.; Wang, C.; Zhang, Y. An enzyme-free electrochemical biosensor based on target-catalytic hairpin assembly and Pd@UiO-66 for the ultrasensitive detection of microRNA-21. *Anal. Chim. Acta* **2020**, *1138*, 59–68. [[CrossRef](#)] [[PubMed](#)]
228. Li, Y.L.; Yu, C.; Yang, B.; Liu, Z.R.; Xia, P.Y.; Wang, Q. Target-catalyzed hairpin assembly and metal-organic frameworks mediated nonenzymatic co-reaction for multiple signal amplification detection of miR-122 in human serum. *Biosens. Bioelectron.* **2018**, *102*, 307–315. [[CrossRef](#)]
229. Wu, C.; Wu, X.; Hou, F.; Wu, L.; Liu, G. An ultrasensitive electrochemical aptasensor based on Pd@PCN-222 as a signal probe coupled with exonuclease III-assisted cycling amplification for the detection of ochratoxin A. *Food Control* **2022**, *139*, 109066–109074. [[CrossRef](#)]
230. Ling, P.; Lei, J.; Jia, L.; Ju, H. Platinum nanoparticles encapsulated metal-organic frameworks for the electrochemical detection of telomerase activity. *Chem. Commun.* **2016**, *52*, 1226–1229. [[CrossRef](#)]
231. Yu, Y.J.; Yu, C.; Niu, Y.Z.; Chen, J.; Zhao, Y.L.; Zhang, Y.C.; Gao, R.F.; He, J.L. Target triggered cleavage effect of DNAzyme: Relying on Pd-Pt alloys functionalized Fe-MOFs for amplified detection of Pb<sup>2+</sup>. *Biosens. Bioelectron.* **2018**, *101*, 297–303. [[CrossRef](#)] [[PubMed](#)]
232. Duan, Y.; Wang, N.; Huang, Z.; Dai, H.; Xu, L.; Sun, S.; Ma, H.; Lin, M. Electrochemical endotoxin aptasensor based on a metal-organic framework labeled analytical platform. *Mater. Sci. Eng. C Mater. Biol. Appl.* **2020**, *108*, 110501–110507. [[CrossRef](#)] [[PubMed](#)]
233. Liu, J.B.; Shang, Y.H.; Zhu, Q.Y.; Zhang, X.X.; Zheng, J.B. A voltammetric immunoassay for the carcinoembryonic antigen using silver(i)-terephthalate metal-organic frameworks containing gold nanoparticles as a signal probe. *Microchim. Acta* **2019**, *186*, 509–516. [[CrossRef](#)] [[PubMed](#)]
234. Yang, X.; Lv, J.J.; Yang, Z.H.; Yuan, R.; Chai, Y.Q. A sensitive electrochemical aptasensor for thrombin detection based on electroactive Co-based metal-organic frameworks with target-triggering nesa strategy. *Anal. Chem.* **2017**, *89*, 11636–11640. [[CrossRef](#)]
235. Wang, H.; Jian, Y.N.; Kong, Q.K.; Liu, H.Y.; Lan, F.F.; Liang, L.L.; Ge, S.G.; Yu, J.H. Ultrasensitive electrochemical paper-based biosensor for microRNA via strand displacement reaction and metal-organic frameworks. *Sens. Actuators B Chem.* **2018**, *257*, 561–569. [[CrossRef](#)]
236. Zhou, C.; Cui, K.; Liu, Y.; Hao, S.; Zhang, L.; Ge, S.; Yu, J. Ultrasensitive microfluidic paper-based electrochemical/visual analytical device via signal amplification of Pd@hollow Zn/Co core-shell ZIF67/ZIF8 nanoparticles for prostate-specific antigen detection. *Anal. Chem.* **2021**, *93*, 5459–5467. [[CrossRef](#)]
237. Li, D.-I.; Zhang, X.; Ma, Y.; Deng, Y.; Hu, R.; Yang, Y. Preparation of an OTA aptasensor based on a metal-organic framework. *Anal. Methods* **2018**, *10*, 3273–3279. [[CrossRef](#)]
238. Liu, J.L.; Ma, Y.C.; Yang, T.; Hu, R.; Yang, Y.H. A single nucleotide polymorphism electrochemical sensor based on DNA-functionalized Cd-MOFs-74 as cascade signal amplification probes. *Microchim. Acta* **2021**, *188*, 266–275. [[CrossRef](#)]

239. Liu, H.; Wang, J.; Jin, H.; Wei, M.; Ren, W.; Zhang, Y.; Wu, L.; He, B. Electrochemical biosensor for sensitive detection of Hg<sup>2+</sup> based on clustered peonylike copper-based metal-organic frameworks and DNAzyme-driven DNA walker dual amplification signal strategy. *Sens. Actuators B Chem.* **2021**, *329*, 129215–129224. [[CrossRef](#)]
240. Xie, F.-T.; Li, Y.-L.; Guan, Y.; Liu, J.-W.; Yang, T.; Mao, G.-J.; Wu, Y.; Yang, Y.-H.; Hu, R. Ultrasensitive dual-signal electrochemical ratiometric aptasensor based on Co-MOFs with intrinsic self-calibration property for Mucin 1. *Anal. Chim. Acta* **2022**, *1225*, 340219–340227. [[CrossRef](#)]
241. Liu, T.Z.; Hu, R.; Zhang, X.; Zhang, K.L.; Liu, Y.; Zhang, X.B.; Bai, R.Y.; Li, D.; Yang, Y.H. Metal-organic framework nanomaterials as novel signal probes for electron transfer mediated ultrasensitive electrochemical immunoassay. *Anal. Chem.* **2016**, *88*, 12516–12523. [[CrossRef](#)] [[PubMed](#)]
242. Dong, J.; Zhang, D.; Li, C.; Bai, T.; Jin, H.; Suo, Z. A sensitive electrochemical sensor based on PtNPs@Cu-MOF signal probe and DNA walker signal amplification for Pb<sup>2+</sup> detection. *Bioelectrochemistry* **2022**, *146*, 108134–108141. [[CrossRef](#)] [[PubMed](#)]
243. Chen, Y.; Meng, X.Z.; Gu, H.W.; Yi, H.C.; Sun, W.Y. A dual-response biosensor for electrochemical and glucometer detection of DNA methyltransferase activity based on functionalized metal-organic framework amplification. *Biosens. Bioelectron.* **2019**, *134*, 117–122. [[CrossRef](#)] [[PubMed](#)]
244. Yang, J.; Dong, P.; Wang, Y.; Liu, T.; Huang, Y.; Lei, J. A stepwise recognition strategy for the detection of telomerase activity via direct electrochemical analysis of metal-organic frameworks. *Analyst* **2021**, *146*, 1859–1864. [[CrossRef](#)]
245. Li, Z.Y.; Li, Y.; Huang, L.; Hu, R.; Yang, T.; Yang, Y.H. An electrochemical aptasensor based on intelligent walking DNA nanomachine with cascade signal amplification powered by nuclease for Mucin 1 assay. *Anal. Chim. Acta* **2022**, *1214*, 339964–339971. [[CrossRef](#)]
246. Dong, J.; Wen, L.; Yang, H.; Zhao, J.; He, C.; Hu, Z.; Peng, L.; Hou, C.; Huo, D. Catalytic hairpin assembly-driven ratiometric dual-signal electrochemical biosensor for ultrasensitive detection of MicroRNA based on the ratios of Fe-MOFs and MB-GA-UiO-66-NH<sub>2</sub>. *Anal. Chem.* **2022**, *94*, 5846–5855. [[CrossRef](#)]
247. Xie, F.T.; Zhao, X.L.; Chi, K.N.; Yang, T.; Hu, R.; Yang, Y.H. Fe-MOFs as signal probes coupling with DNA tetrahedral nanostructures for construction of ratiometric electrochemical aptasensor. *Anal. Chim. Acta* **2020**, *1135*, 123–131. [[CrossRef](#)]
248. Li, Z.; Dai, G.; Luo, F.; Lu, Y.; Zhang, J.; Chu, Z.; He, P.; Zhang, F.; Wang, Q. An electrochemical sensor for bacterial lipopolysaccharide detection based on dual functional Cu<sup>2+</sup>-modified metal-organic framework nanoparticles. *Microchim. Acta* **2020**, *187*, 415–424. [[CrossRef](#)]
249. Yiwei, X.; Yahui, L.; Weilong, T.; Jiyong, S.; Xiaobo, Z.; Wen, Z.; Xinai, Z.; Yanxiao, L.; Changqiang, Z.; Lele, A.; et al. Electrochemical determination of hantavirus using gold nanoparticle-modified graphene as an electrode material and Cu-based metal-organic framework assisted signal generation. *Microchim. Acta* **2021**, *188*, 112–121. [[CrossRef](#)]
250. Zhang, C.; Zhang, D.; Ma, Z.; Han, H. Cascade catalysis-initiated radical polymerization amplified impedimetric immunosensor for ultrasensitive detection of carbohydrate antigen 15-3. *Biosens. Bioelectron.* **2019**, *137*, 1–7. [[CrossRef](#)]
251. Dong, H.B.; Hu, X.J.; Zhao, J.L.; Li, H.J.; Koh, K.; Gao, L.; Shao, M.; Chen, H.X. Sensitive detection of fractalkine based on AuNPs and metal-organic frameworks composite at para-sulfonatocalix 4 arene-AuNPs assembled multilayer interface. *Sens. Actuators B Chem.* **2018**, *276*, 150–157. [[CrossRef](#)]
252. Shen, W.J.; Zhuo, Y.; Chai, Y.Q.; Yuan, R. Ce-based metal-organic frameworks and DNAzyme-assisted recycling as dual signal amplifiers for sensitive electrochemical detection of lipopolysaccharide. *Biosens. Bioelectron.* **2016**, *83*, 287–292. [[CrossRef](#)] [[PubMed](#)]
253. Yu, H.; Han, J.; An, S.J.; Xie, G.; Chen, S.P. Ce(III, IV)-MOF electrocatalyst as signal-amplifying tag for sensitive electrochemical aptasensing. *Biosens. Bioelectron.* **2018**, *109*, 63–69. [[CrossRef](#)] [[PubMed](#)]
254. Dong, P.; Zhu, L.; Huang, J.; Ren, J.; Lei, J. Electrocatalysis of cerium metal-organic frameworks for ratiometric electrochemical detection of telomerase activity. *Biosens. Bioelectron.* **2019**, *138*, 111313–111320. [[CrossRef](#)]
255. Ling, P.; Lei, J.; Ju, H. Nanoscaled porphyrinic metal-organic frameworks for electrochemical detection of telomerase activity via telomerase triggered conformation switch. *Anal. Chem.* **2016**, *88*, 10680–10686. [[CrossRef](#)]
256. Ling, P.; Lei, J.; Ju, H. Porphyrinic metal-organic framework as electrochemical probe for DNA sensing via triple-helix molecular switch. *Biosens. Bioelectron.* **2015**, *71*, 373–379. [[CrossRef](#)]
257. Song, W.; Yin, W.; Zhang, Z.; He, P.; Yang, X.; Zhang, X. A DNA functionalized porphyrinic metal-organic framework as a peroxidase mimicking catalyst for amperometric determination of the activity of T4 polynucleotide kinase. *Microchim. Acta* **2019**, *186*, 149–156. [[CrossRef](#)]
258. Zhang, G.; Shan, D.; Dong, H.; Cosnier, S.; Al-Ghanim, K.A.; Ahmad, Z.; Mahboob, S.; Zhang, X. DNA-mediated nanoscale metal-organic frameworks for ultrasensitive photoelectrochemical enzyme-free immunoassay. *Anal. Chem.* **2018**, *90*, 12284–12291. [[CrossRef](#)]
259. Zhang, X.; Wasson, M.C.; Shayan, M.; Berdichevsky, E.K.; Ricardo-Noordberg, J.; Singh, Z.; Papazyan, E.K.; Castro, A.J.; Marino, P.; Ajoyan, Z.; et al. A historical perspective on porphyrin-based metal-organic frameworks and their applications. *Coord. Chem. Rev.* **2021**, *429*, 213615–213636. [[CrossRef](#)]
260. Cui, L.; Wu, J.; Li, J.; Ju, H. Electrochemical sensor for lead cation sensitized with a DNA functionalized porphyrinic metal-organic framework. *Anal. Chem.* **2015**, *87*, 10635–10641. [[CrossRef](#)]

261. Bao, T.; Fu, R.; Jiang, Y.; Wen, W.; Zhang, X.; Wang, S. Metal-mediated polydopamine nanoparticles-DNA nanomachine coupling electrochemical conversion of metal-organic frameworks for ultrasensitive MicroRNA sensing. *Anal. Chem.* **2021**, *93*, 13475–13484. [[CrossRef](#)] [[PubMed](#)]
262. He, W.; Ifraemov, R.; Raslin, A.; Hod, I. Room-temperature electrochemical conversion of metal-organic frameworks into porous amorphous metal sulfides with tailored composition and hydrogen evolution activity. *Adv. Funct. Mater.* **2018**, *28*, 1707244–1707252. [[CrossRef](#)]
263. Guo, L.; Mu, Z.; Yan, B.; Wang, J.; Zhou, J.; Bai, L. A novel electrochemical biosensor for sensitive detection of non-small cell lung cancer ctDNA using NG-PEI-COFTAPB-TFPB as sensing platform and Fe-MOF for signal enhancement. *Sens. Actuators B Chem.* **2022**, *350*, 130874–130883. [[CrossRef](#)]
264. Tang, J.; Liu, L.; Qin, J.; Lv, X.; Li, J.; Tang, D.; Zhuang, J. Biocatalysis-mediated MOF-to-prussian blue transformation enabling sensitive detection of NSCLC-associated miRNAs with dual-readout signals. *Biosens. Bioelectron.* **2022**, *206*, 114139–114147. [[CrossRef](#)] [[PubMed](#)]
265. Song, Z.; Li, Y.; Teng, H.; Ding, C.; Xu, G.; Luo, X. Designed zwitterionic peptide combined with sacrificial Fe-MOF for low fouling and highly sensitive electrochemical detection of T4 polynucleotide kinase. *Sens. Actuators B Chem.* **2020**, *305*, 127329–127337. [[CrossRef](#)]